






Functional variation among LPMOs revealed by the inhibitory effects of cyanide and buffer ions

Ole Golten¹ , Lorenz Schwaiger², Zarah Forsberg¹ , Kelsi R. Hall^{1,3}, Anton A. Stepnov¹ , Tom Z. Emrich-Mills¹, Iván Ayuso-Fernández^{1,4}, Morten Sørli¹ , Roland Ludwig² , Åsmund Kjendseth Røhr¹ and Vincent G. H. Eijsink¹

¹ Faculty of Chemistry, Biotechnology and Food Science, Norwegian University of Life Sciences (NMBU), Ås, Norway

² Department of Food Science and Technology, Institute of Food Technology, University of Natural Resources and Life Sciences, Vienna, Austria

³ School of Biological Sciences, University of Canterbury, Christchurch, New Zealand

⁴ Biotechnology Department, Margarita Salas Center for Biological Research (CIB-CSIC), Madrid, Spain

Correspondence

Vincent G. H. Eijsink, Faculty of Chemistry, Biotechnology and Food Science, Norwegian University of Life Sciences (NMBU), P.O. box 5003, 1430 Ås, Norway
Tel: +47 67232463
E-mail: vincent.eijsink@nmbu.no

(Received 14 November 2024, revised 23 December 2024, accepted 9 January 2025, available online 6 February 2025)

doi:10.1002/1873-3468.15105

Edited by Peter Brzezinski

Enzymes known as lytic polysaccharide monooxygenases (LPMOs) are mono-copper polysaccharide-degrading peroxygenases that engage in several on- and off-pathway redox reactions involving O₂ and H₂O₂. Herein, we show that the known metalloenzyme inhibitor cyanide inhibits reductive activation of LPMOs by binding to the LPMO-Cu(II) state and that the degree of inhibition depends on the concentrations of the polysaccharide substrate, the reductant and H₂O₂. Importantly, this analysis revealed differences between fungal *NcAA9C* and bacterial *SmAA10A*, which have different secondary copper coordination spheres. These differences were also highlighted by the observation that phosphate, a commonly used buffer ion, strongly inhibits *NcAA9C* while not affecting reactions with *SmAA10A*. The results provide insight into LPMO inhibition and catalysis and highlight pitfalls in the analysis thereof.

Keywords: cellulose; chitin; copper; cyanide; LPMO; lytic polysaccharide monooxygenase

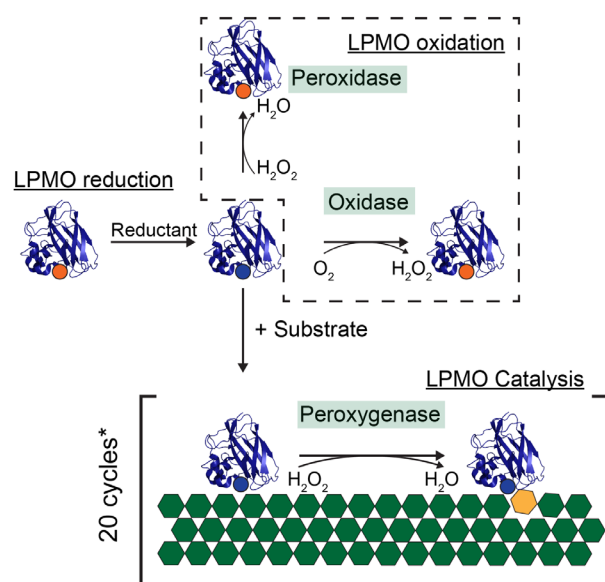
Lytic polysaccharide monooxygenases (LPMOs) are mono-nuclear copper enzymes capable of activating C-H bonds with bond dissociation energies close to 100 kcal·mol⁻¹ [1] and have received substantial interest due to their fascinating chemistry [2,3] and relevance in industry [4–6]. Since their discovery [7,8], LPMOs have been identified in several phyla of life and their (putative) roles today include roles in biomass degradation [9,10], bacterial, fungal, and oomycete pathogenicity [11–14], insect molting [15] and bacterial cell wall remodeling [16]. The copper ion is

coordinated by a highly conserved histidine brace [2,17], while amino acids in the immediate vicinity of this brace, i.e., the second coordination sphere, tune copper reactivity [18–21]. Currently, based on their sequences, LPMOs are classified into eight families of Auxiliary Activities (AA) in the carbohydrate-active enzyme database (CAZy) [22].

While LPMOs show functional variation, for example, in terms of substrate specificity and oxidative regioselectivity [7,23–30], they all appear to engage in a similar set of interrelated on- and off-pathway

Abbreviations

AA, auxiliary activity; Bis-Tris, 2-[Bis-(2-hydroxyethyl)-amino]-2-hydroxymethyl-propane-1,3-diol; CAZy, Carbohydrate-active enzyme database; EPR, Electron paramagnetic resonance; KMSA, potassium methanesulfonate; LPMO, lytic polysaccharide monooxygenase; MOPS, 3-N(morpholino)propanesulfonic acid; SHE, standard hydrogen electrode; Tris/HCl, Tris(hydroxymethyl)aminomethane hydrochloride.



reactions (Fig. 1). It has been challenging to unravel these reactions, partly due to initial confusion surrounding the co-substrate. Initially, LPMOs were thought to be monooxygenases ($\text{R-H} + \text{O}_2 + 2\text{e}^- + 2\text{H}^+ \rightarrow \text{R-OH} + 2\text{H}_2\text{O}$), using O_2 as a co-substrate [7,17,33]. However, recent work has shown that LPMOs are peroxygenases ($\text{R-H} + \text{H}_2\text{O}_2 \rightarrow \text{R-OH} + \text{H}_2\text{O}$) using H_2O_2 as the co-substrate [27,34–38]. Confusingly, in reactions run under “monooxygenase conditions” (i.e., LPMO + substrate + reductant, aerobic conditions), hereafter referred to as *in situ* H_2O_2 -limiting conditions, H_2O_2 is generated *in situ* through the LPMO oxidase activity [39] and abiotic oxidation of the reductant [40,41]. Thus, it has been claimed that most, if not all, observed apparent monooxygenase reactions, are peroxygenase reactions limited by the rate of *in situ* generation of H_2O_2 .

abiotic oxidation of commonly used reductants such as ascorbate, thus affecting the *in situ* generation of H_2O_2 [41]. In addition, oxidative damage to LPMOs will lead to the release of copper from the active site, meaning that free copper levels, and thus the levels of *in situ* generated H_2O_2 , vary as the reaction proceeds [41,42]. The combination of the latter two effects can make LPMO inactivation a self-reinforcing process [43]. Finally, the contribution of the oxidase reaction to the *in situ* generation of H_2O_2 varies between LPMOs [44]. Running reactions with externally added H_2O_2 or controlled *in situ* generation of H_2O_2 with enzymes like glucose oxidase can overcome these complications to some extent [6,27,34].

The issues discussed above are also relevant when assessing LPMO inhibitors, while, at the same time, the use of inhibitors can shed light on LPMO catalysis. So far, little is known about LPMO inhibition, and available studies have focused on natural organic inhibitors [45,46], organic acids, and amino acids [47]. The solvent-exposed copper can be affected by known inhibitors of copper enzymes, such as cyanide [48,49], and, indeed, early studies done before the discovery of the peroxygenase activity of LPMOs showed that cyanide inhibits the bacterial chitin-active LPMO *SmAA10A* [7]. Cyanide is an interesting LPMO inhibitor since Cu-CN complexes may mimic some of the possible copper-oxo species generated during on- or off-pathway catalysis, in particular, the Cu-superoxide complex that likely emerges when a reduced LPMO reacts with molecular oxygen [50]. Such mimicking is less likely for the peroxygenase reaction, which depends on the homolytic cleavage of H_2O_2 at the Cu(I) active site, yielding a copper-hydroxide (Cu(II)-OH) and a hydroxyl radical, OH^\bullet . While the next reaction step remains enigmatic, it has been repeatedly proposed that a copper-oxyl (Cu(II)- O^\bullet) is formed, which performs the hydrogen atom abstraction from the substrate [18,35,51,52].

In this work, we have probed the effect of cyanide on LPMOs during on- and off-pathway turnover. By gauging the effect of cyanide on both the productive reaction and off-pathway reactions, we provide insight into the impact of substrate and reductant concentrations, and we unveil principles and pitfalls of interpreting LPMO reaction kinetics. Importantly, our studies, which include an assessment of the impact of buffer ions, reveal important differences between the two studied LPMOs, fungal *NcAA9C* and bacterial *SmAA10A* (Fig. 2A). To the best of our knowledge, this work is the first LPMO inhibition study that assesses inhibitory effects on product formation in reactions with natural LPMO substrates over time.

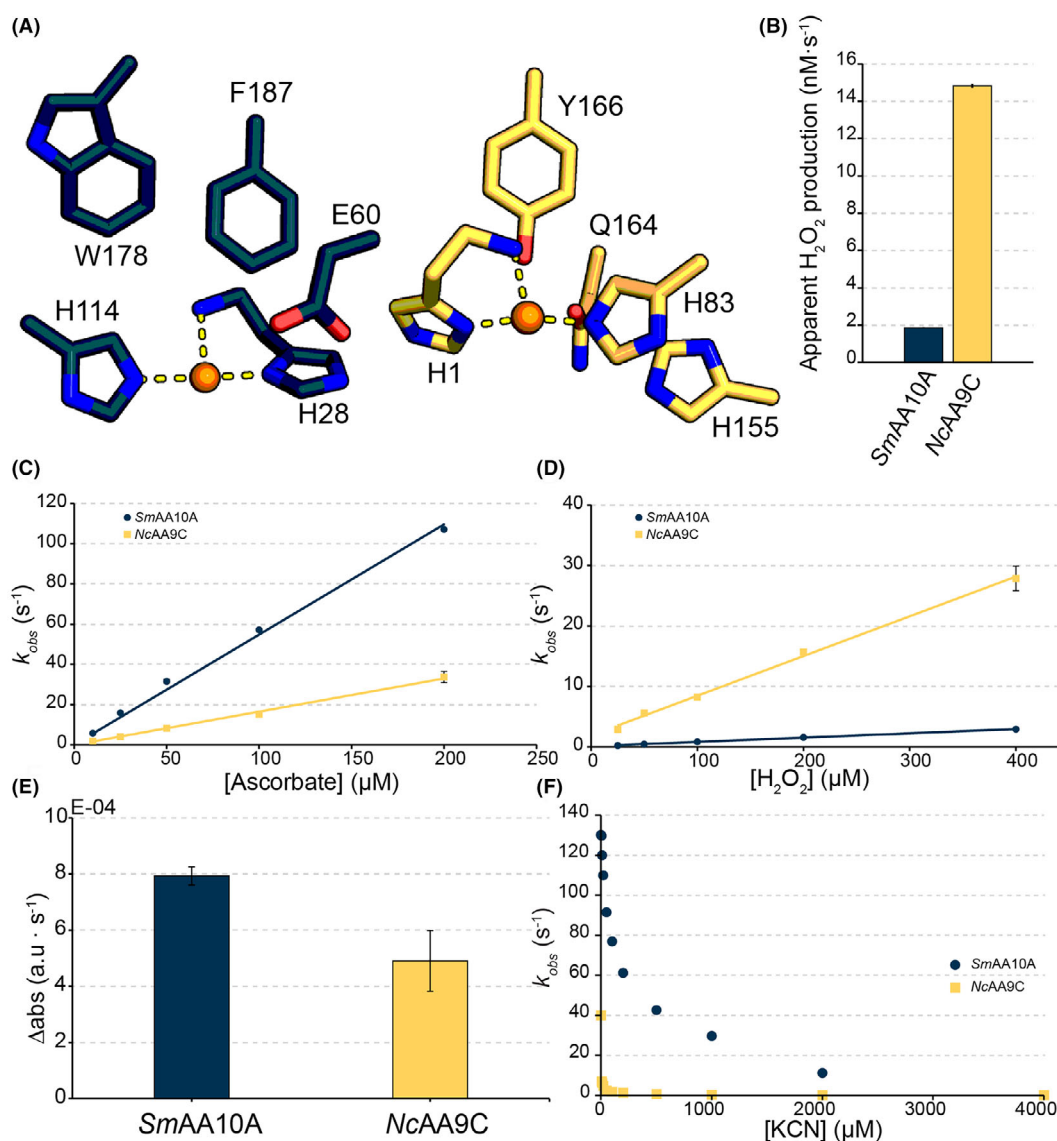


Fig. 2. Comparison of copper reactivity in *SmAA10A* and *NcAA9C*. (A) Structural comparison of the active sites of *SmAA10A* and *NcAA9C* showing the conserved histidine brace and selected second sphere residues. (B) Oxidase activity of 1 μM *SmAA10A* and *NcAA9C* reacting with 1 mM ascorbate at 30 °C. (C) Pseudo-first-order reduction rates (k_{obs}) with increasing concentrations of ascorbate (10–200 μM). (D) Pseudo-first-order LPMO oxidation rates (k_{obs}) with increasing concentrations of H_2O_2 (25–400 μM). (E) Initial rates of 2,6-DMP oxidation in reactions with 2 μM enzyme, 1 mM 2,6-DMP and 50 μM H_2O_2 . All reactions were done in 50 mM MOPS, pH 7.0, in triplicates. Standard deviations are shown as error bars. (F) Pseudo-first-order reduction rates (k_{obs}) in reactions with 200 μM ascorbate and varying amounts of cyanide (0–4000 μM). The increased apparent reduction rate observed in the reaction with 200 μM ascorbate and no cyanide (compared to panel C) results from the increased instrument dead time in the required double mixing setup, meaning that the entire single exponential cannot be measured.

Materials and methods

Materials

All chemicals were sourced from Sigma-Aldrich if not stated otherwise. β -chitin was sourced from France Chitin, Orange, France, batch number 20140101 and milled to a particle size of

75–200 μm using a PM 200 planetary ball mill (Retsch, Haan, Germany) equipped with zirconium oxide milling tools. Aliquots of ascorbate were prepared at a 100 mM concentration in TraceSELECT™ water (Honeywell, Charlotte, NC, USA) before storing at -20 °C until use. All reactions containing cyanide were prepared using potassium cyanide. Cyanide

stocks were prepared fresh by dissolving potassium cyanide in 0.5 M 3-N(morpholino)propanesulfonic acid (MOPS) pH 7.0 and diluting with 50 mM MOPS pH 7.0 immediately before use. H₂O₂ stock solutions were prepared fresh, and the concentration was verified by measuring the absorbance at 240 nm using an extinction coefficient of 43.6 cm⁻¹·M⁻¹.

Enzyme expression and purification

The chitinolytic AA10 LPMO from *Serratia marcescens* (*SmAA10A*; also known as CBP21) was expressed and purified as previously described using hydrophobic interaction chromatography with a chitin bead column [8].

The fungal LPMO from *Neurospora crassa* (*NcAA9C*) was expressed and purified as previously described using a combination of hydrophobic interaction and anion-exchange chromatography [39,53].

Copper saturation

To ensure copper saturation, the purified enzymes were incubated with a 3-fold molar excess of CuSO₄ for 30–60 min at 4 °C in 50 mM Tris(hydroxymethyl)aminomethane hydrochloride (Tris/HCl) pH 8.0, followed by removal of excess free copper. Two methods for removal of free copper were used. For *SmAA10A*, a series of concentration and dilution steps using 50 mM Tris/HCl, pH 8.0, were performed using the 10 kDa Amicon® Ultra-15 centrifugal filter unit (Merck, Darmstadt, Germany) to reach a minimum dilution factor of 1 000 000-fold. For *NcAA9C*, a HiPrep 26/10 desalting column was used to remove the excess free copper and change the buffer to 50 mM Tris/HCl, pH 7.0, and 100 mM NaCl. In both cases, the enzyme preparations were controlled for excess free copper by monitoring the (absence of) copper-mediated oxidation of ascorbate in an ultrafiltrate of the final enzyme preparation, using the Amplex Red/horseradish peroxidase reaction as previously described [39,41].

LPMO oxidase activity

The oxidase activity was measured using a protocol adapted from [39,54]. In brief, 90 µL of a reaction mixture containing 50 mM MOPS, pH 7.0, 0.1 mM Amplex Red (AR), 5 U·mL⁻¹ horse radish peroxidase (HRP) and 1 mM ascorbate was incubated for 5 min at 30 °C before adding 10 µL of enzyme to a final concentration of 1 µM for *NcAA9C* and 3 µM *SmAA10A*. The production of H₂O₂ was monitored at 542 nm over 20 min, and the initial rate was determined from the linear portion of the product formation curve.

Chitin degradation by *SmAA10A*

Reactions with *SmAA10A* were performed by mixing 1 µM enzyme, 50 mM MOPS, pH 7.0, and β-chitin (0.5–10 g·L⁻¹) for a 30 min pre-incubation at 30 °C with 850 rpm agitation

in a ThermoMixer Comfort (Thermo Fisher Scientific, Waltham, MA, USA). The reactions were then initiated by adding ascorbate to a final concentration of 25–1000 µM. In reactions with exogenously added H₂O₂, the H₂O₂ was added to a final concentration of 100 µM immediately before the addition of ascorbate. For reactions containing cyanide, cyanide from a concentrated stock solution was added at the 15-min mark during the pre-incubation of the enzyme with the substrate.

The reactions were terminated at different time points by filtering 75 µL aliquots through a 0.45 µm MultiScreen™ 96-well filter plate (Merck). The filtrates were incubated with 1 µM chitinase (*SmCHB*) for 16 h at 37 °C to degrade the solubilized oxidized chitooligomers to the oxidized dimer (chitobionic acid, GlcNAcGlcNAc1A) and the native monomer (GlcNAc), which simplifies analysis and product quantification.

To determine the total amount of oxidized products, 75 µL sample aliquots were transferred to microtubes, followed by enzyme inactivation through boiling for 10 min. The samples were cooled and then diluted two-fold before adding 1 µM Chitinase A from *Serratia marcescens* (*SmChiA*) and 1 µM *SmCHB*, followed by incubation at 40 °C for 24 h.

Substrate degradation by *NcAA9C*

NcAA9C reactions were performed by incubating 1 µM enzyme, 50 mM MOPS, pH 7.0, and cellopentaose (25–1000 µM) (Megazyme, Bray, Ireland) or 0.1% (w/v) phosphoric acid swollen cellulose (PASC), prepared from Avicel according to [55], for a 30 min pre-incubation at 30 °C with 850 rpm agitation in a ThermoMixer Comfort (Thermo Fisher Scientific). The reactions were initiated by adding 25–1000 µM ascorbate. In reactions with exogenously added H₂O₂, the H₂O₂ was added to a final concentration of 100 µM immediately before adding ascorbate. For reactions containing cyanide, cyanide from a concentrated stock was added at the 15-min mark during the pre-incubation of enzyme with the substrate.

For reactions performed with cellopentaose, 25 µL samples were taken at varying timepoints, which were diluted 10-fold in 200 mM NaOH, to terminate the reaction, followed by filtering through a 0.45 µm MultiScreen™ 96-well filter plate (Merck).

Reactions with PASC were terminated by sampling 65 µL at various time points, followed by boiling for 10 min, and filtering through a 0.45 µm MultiScreen™ 96-well filter plate (Merck).

HPLC analysis of chitin-derived products

Analysis of chitobionic acid and the native monomer was performed using an Ultimate 3000 RSLC UHPLC (Dionex, Sunnyvale, CA, USA) by injecting an 8 µL sample onto a 100 × 7.8 Rezex RFQ-Fast acid H+ (8%) column

(Phenomenex, Torrance, CA, USA) operated at 85 °C with a flow rate of 1 mL·min⁻¹. An isocratic gradient of 5 mM sulfuric acid was used. Products were detected by UV at 194 nm and chitobionic acid was quantified using in-house generated standards (25–1600 µM) as previously described [12,56].

Since ascorbate co-elutes with chitobionic acid, an alternative analytical method was used for experiments involving various concentrations of ascorbate, involving an Agilent 1290 Infinity II UHPLC (Agilent, Santa Clara, CA, USA) equipped with a 2.1 × 50 mm, 130 Å, 1.7 µm BEH Amide column (Waters, Milford, MA, USA) and a 5 mm VanGuard pre-column with the same column material. The analysis was performed by injecting a 5 µL sample with a flow rate of 0.4 mL·min⁻¹ at 25 °C followed by isocratic elution with 78% acetonitrile and 22% 15 mM Tris/HCl, pH 8.0. All samples were adjusted to 78% (v/v) acetonitrile before injection.

HPLC analysis of cellulose-derived products

Products generated from PASC or cellopentaose were analyzed using High Performance Anion Exchange Chromatography with Pulsed Amperometric Detection (HPAEC-PAD) on an ICS 6000 (Dionex) equipped with a 1 × 250 mm CarboPac PA200 (Thermo Fisher Scientific) column and a 1 × 50 mm guard column of the same material, as described before [57]. The flow rate was 62 µL · min⁻¹, and the column oven temperature was 30 °C.

For quantification of the native trimer, a 27-min method was used with a dual eluent generator creating the KOH and potassium methanesulfonate (KMSA) eluents, with the following gradient: 0–30 mM KMSA over 0–6 min; 30–100 mM KMSA over 4 min and held for an additional 5 min; 100–0 mM KMSA over 0.1 min; 0 mM KMSA held for 11.9 min. The KOH concentration remained fixed at 100 mM throughout the run. Quantification of the native trimer was performed using purchased cellotriose as a standard (Megazyme).

For quantification of C4-oxidized products, a 26-min method was used with the following gradient: 1–100 mM KMSA over 14 min and held for an additional 3 min; 100–1 mM KMSA over 0.1 min; 1 mM KMSA for 8.9 min. The KOH concentration remained fixed at 100 mM throughout the run. Quantification of the C4-oxidized dimer and trimer was performed using in-house generated standards as previously described [57].

Transient state stopped-flow kinetics

The transition between LPMO-Cu(II) and LPMO-Cu(I) in both the presence and absence of cyanide was analyzed using a SFM 4000 stopped-flow equipped with a MOS 200 M dual absorbance spectrofluorometer (BioLogic, Seyssinet-Pariset, France). To ensure single turnover

conditions, all reactions were performed anaerobically by storing N₂ purged buffer and labware in an A95TG anaerobic workstation (Don Whitley, West Yorkshire, UK) for 16 h before usage. Enzyme, ascorbate, and cyanide solutions were prepared fresh in the chamber and sealed in syringes before transferring to the stopped-flow syringe handling unit, which had been flushed with N₂ purged buffer. For determining reduction and oxidation rates, the fluorescence shift between LPMO-Cu(II) and LPMO-Cu(I) [58] was monitored using a PMT-250 photomultiplier tube (BioLogic) with a set voltage of 600 V.

For reactions without cyanide, the reduction was assessed by a single mixing experiment, mixing 5 µM LPMO-Cu(II) with increasing concentrations of ascorbate (10–200 µM) in 50 mM MOPS, sodium phosphate, Tris/HCl or 2-[Bis-(2-hydroxyethyl)-amino]-2-hydroxymethyl-propane-1,3-diol (Bis-Tris), pH 7.0. In reactions with cyanide and when measuring LPMO oxidation, we used a double mixing setup with a 100 µL delay line. For reduction in the presence of cyanide, 5 µM LPMO-Cu(II) was mixed with an equal volume of solutions with increasing concentrations of cyanide (10–2000 µM) and stored in the delay line for 10 s, followed by a second mixing with 200 µM ascorbate.

For reoxidation experiments, 10 µM LPMO-Cu(II) was mixed with equimolar amounts of L-cysteine and stored for 10 s in the delay line to ensure reduction before mixing with increasing concentrations of H₂O₂ (10–800 µM). These experiments were performed in 50 mM MOPS, pH 7.0.

For all cases, the pseudo-first order reaction rates (k_{obs}) were determined by solving a baseline corrected single exponential equation ($y = at + b + ce^{-k_{\text{obs}}t}$).

Monitoring of H₂O₂ consumption with an electrochemical sensor

To monitor the real-time consumption of H₂O₂, a Prussian blue-coated rotating disk gold electrode was used as described in [27]. In short, the electrochemical setup consisted of a rotating disk gold working electrode, a double junctioned Ag/AgCl reference electrode with a 3 M KCl supporting electrolyte and an in-house customized platinum sheet counter electrode. To selectively react with H₂O₂, the gold working electrode was modified by electro-depositing a thin layer of Prussian blue, which was achieved by performing 6–8 cycles of staircase cyclic voltammetry, applying a potential scan between 600 and 900 mV vs standard hydrogen electrode (SHE) in a solution of 0.1 M KCl, 1 mM K₃[Fe(CN)₆], 1 mM FeCl₃ and 0.1 M HCl. After the Prussian blue deposition, the working electrode was activated in 0.1 M KCl and 0.1 M HCl by performing 20 cyclic voltammetry staircase scans between 160 and 590 mV vs SHE. Only working electrodes obtaining anodic peak densities between 2 and 4 nA·cm⁻² during activation were used. After activation, the gold electrode was covered with a layer of Nafion™ (5% in aliphatic alcohols, Merck) by

pipetting 7 μL undiluted Nafion onto the electrode surface and cured overnight to protect the Prussian blue coating from abrasion during later use. Before analysis, the working electrode was activated in the buffer used for analysis with 0.1 M KCl by performing 20 CV staircase scans between 160 and 590 mV vs SHE.

Reactions with *NcAA9C* were performed with 4 g·L⁻¹ tamarind seed xyloglucan (Megazyme) as substrate, while reactions with *SmAA10A* were performed with 10 g·L⁻¹ β -chitin. Both reactions were prepared in 0.1 M KCl and 50 mM buffer, pH 7.0 (MOPS, sodium phosphate, Tris/HCl, or Bis-Tris). Real-time monitoring of H₂O₂ consumption was performed using chronoamperometry by applying a potential of 100 mV vs SHE. A typical reaction was performed using an angular velocity of 50 s⁻¹ and was preceded by an electrode polarization step during which the signal was monitored for 45–60 s to obtain a stable signal. An internal calibration of each run was performed by five consecutive additions of known amounts of H₂O₂ before initiating the LPMO reaction, reaching a total starting concentration of H₂O₂ of either 50 μM (*SmAA10A*) or 100 μM (*NcAA9C*). After this calibration step, the enzyme was added and mixed for approx. 30 s before adding ascorbate (100 μM) to start the LPMO reaction.

H₂O₂ sensor data analysis

With electrochemical detection of H₂O₂ using a rotating disk electrode, the reduction in the H₂O₂ concentration over time is observed as a change in current over time, as thoroughly described in [27]. The raw traces were first corrected for a system drift, which was performed using a two-point linear baseline correction. One point was selected during the electrode polarization (pre-experiment), and the second in the post-experimental baseline. In reactions that terminated prior to consuming all the H₂O₂, the system drift was determined in the post-experimental baseline over a duration of 30–60 s. Following the baseline correction, linear regression was performed on the currents measured during the five-step calibration procedure, yielding the relationship between current, in nano ampere (nA), and the concentration of H₂O₂ in μM . Following the conversion from current to μM H₂O₂, figures were prepared showing only the data points from the reaction start until the reaction, meaning that the figures only show LPMO-related H₂O₂ consumption. All data analysis can be performed using a command line interface, which is available on GitHub (https://github.com/ogo001/H2O2_RDE). A schematic representation of the data analysis is presented in Fig. S1. [27].

Reactions with 2,6-dimethoxyphenol (2,6-DMP)

In the presence of H₂O₂, LPMOs oxidize the chromogen 2,6-DMP in what essentially is a peroxidase reaction, resulting in the reduction of H₂O₂ to water and the formation of the

colored compound coeruleignone that absorbs at 469 nm [59]. To assess inhibition of this peroxidase activity by cyanide or sodium phosphate, reaction mixtures were assembled consisting of 2 μM *SmAA10A* or *NcAA9C* in 50 mM MOPS, pH 7.0, with 1 mM 2,6-DMP and 50 μM H₂O₂. Reactions were performed at 30 °C in triplicate in 50 μL volumes in a 96-well plate. Cyanide (0–1000 μM) or sodium phosphate pH 7.0, (0–500 mM) were added to the reaction mixture from concentrated stock solutions. Reactions were initiated by adding 2 μL of concentrated LPMO solution to 48 μL of a pre-mixed, pre-warmed solution of MOPS, 2,6-DMP, H₂O₂ and inhibitor (cyanide or sodium phosphate), followed by brief mixing. Absorbance was monitored at 473 nm using a Multiskan™ FC microplate photometer (Thermo Fisher Scientific). Measurements were recorded every 1 s for 2 min, starting 10 s after the reactions were initiated. The reported values reflect the initial, linear rate of the increase in absorbance recorded between 10 and 20 s after the initiation of the reaction.

Electron paramagnetic resonance (EPR)

Continuous-wave X-band (~ 9.47 GHz) EPR spectra were collected on a Bruker Magnettech ESR5000 (Bruker, Billerica, MA, USA) using custom-made quartz EPR tubes with an outer diameter of 4 mm. Samples were frozen in liquid nitrogen (77 K). Data was collected at 100 K using a sweep time of 60 s, modulation frequency of 100 kHz, modulation amplitude of 1 mT and microwave power of 10 mW. All spectra were analyzed in Matlab using the EasySpin 6.0.0 package [60].

Detection of hydroxyl radicals

The specific radical trap terephthalic acid will react with OH• to generate 2-hydroxyterephthalic acid which is fluorescent. Using a Varioskan Lux (Thermo Fisher Scientific) in fluorescence mode, the formation of OH• in Fenton-like reactions in various buffers was monitored. The reactions contained 5 μM CuSO₄, 1 mM ascorbate, 100 μM H₂O₂, 100 μM terephthalic acid and 50 mM buffer pH 7.0 (MOPS, Bis-Tris, Tris/HCl or sodium phosphate) and radical formation was monitored for 30 min at 30 °C, using a 312 nm excitation and a 328 nm emission wavelength.

Results

Comparison of *SmAA10A* and *NcAA9C*

SmAA10A, a chitin-active bacterial LPMO [7,8], and *NcAA9C*, a fungal LPMO active on cellulose, cello-oligomers and several hemi-cellulosic glycans [39,61,62] are among the best studied LPMOs. The *SmAA10A* active site displays a trigonal-bipyramidal copper

configuration with phenylalanine (*SmAA10A*; Phe187) in the axial position, whilst *NcAA9C* presents a tetragonal active site with a tyrosine (*NcAA9C*; Tyr166) in the axial position (Fig. 2A). These structural features are reflected in altered copper electronics yielding a more rhombic and a more axial EPR spectrum for *SmAA10A* and *NcAA9C*, respectively [63,64]. Expanding beyond the first coordination sphere, the less conserved second sphere residues partake in modulating copper reactivity but do not directly interact with the copper atom. The importance of second sphere residues for catalysis has been demonstrated in several studies using different experimental approaches [21], including studies of *SmAA10A* [8,18] and *NcAA9C* [19]. Here, we have assessed the differences between these two enzymes in more detail, using identical methods and experimental conditions for both.

Oxidase activity, i.e., LPMO-catalyzed oxidation of a reductant leading to formation of H_2O_2 , was monitored using the Amplex Red/HRP method [39,54] in 50 mM MOPS, pH 7.0, and revealed an almost 10-fold difference in rate (Fig. 2B, 0.002 and 0.015 s^{-1} for *SmAA10A* and *NcAA9C*, respectively). These differences were further analyzed using transient state stopped-flow kinetics to probe the reduction rates with ascorbate (Fig. 2C) and oxidation rates with H_2O_2 (Fig. 2D). *In situ* mixing of LPMO-Cu(II) with increasing ascorbate concentrations performed under anaerobic pseudo-first-order conditions in 50 mM MOPS, pH 7.0, yielded reduction rates of $527\,000 \pm 15\,000\text{ M}^{-1}\cdot\text{s}^{-1}$ for *SmAA10A* and $167\,000 \pm 5700\text{ M}^{-1}\cdot\text{s}^{-1}$ for *NcAA9C* (Fig. 2C). Oxidation of *SmAA10A* and *NcAA9C* by H_2O_2 happened with rates amounting to $7500 \pm 300\text{ M}^{-1}\cdot\text{s}^{-1}$ and $72\,600 \pm 2000\text{ M}^{-1}\cdot\text{s}^{-1}$, respectively (Fig. 2D). Compared to *NcAA9C*, *SmAA10A* has a higher reduction rate and a lower LPMO oxidation rate with both O_2 (oxidase assay) and H_2O_2 (stopped-flow data), which aligns with *SmAA10A* having a more positive reduction potential [$275 \pm 6\text{ mV}$ vs SHE [65], pH 7.0, vs $211 \pm 2\text{ mV}$ vs SHE for *NcAA9C* [19], pH 6.5]. The two enzymes showed similar activities in the peroxidase assay with 2,6-DMP (Fig. 2E). The rate of formation of the final product in this reaction depends on two rates, the rate of LPMO reduction by 2,6-DMP and the rate of LPMO oxidation by H_2O_2 [59]. The rate of reduction is higher for *SmAA10A* (when measured with ascorbate) whilst the rate of oxidation by H_2O_2 is higher for *NcAA9C*, which may explain why the two enzymes show similar overall rates.

The effects of cyanide on LPMO reduction rates were then studied to gain more insight into the reduction kinetics.

Strikingly, the reduction of *NcAA9C* was severely inhibited by cyanide, showing almost full inhibition when using equimolar amounts of cyanide (Fig. 2F, yellow squares). Reduction of *SmAA10A* was also clearly inhibited by cyanide, but inhibition was less severe as 2 mM cyanide did not fully inhibit *SmAA10A* (Fig. 2F, blue bullets). The results reveal a difference between the two LPMOs and suggest that cyanide binds to Cu(II), thus competing with the reductant and preventing reduction. Control reactions showed that exposure to cyanide does not affect the fluorescence signal used to monitor LPMO reduction (Fig. S2). Another control experiment without a reductant showed that cyanide cannot drive the LPMO reaction (Fig. S3). Both control experiments also show that cyanide is unable to reduce the LPMO.

EPR spectroscopy

EPR spectroscopy is well suited for the Cu(II) active site due to the d^9 electronic configuration yielding a paramagnetic system, whereas the Cu(I) d^{10} electronic configuration is EPR silent. Using a continuous-wave (CW) X-band EPR spectrometer, the spectra of the LPMOs, alone or with a five-fold molar excess of cyanide, were collected (Fig. 3).

The *SmAA10A* EPR spectrum in the absence of cyanide is rhombic ($g_x \neq g_y \neq g_z$), in line with the trigonal-bipyramidal active site configuration observed for chitin-active AA10 LPMOs with an axial phenylalanine [66,67]. The successful simulation of the *SmAA10A* spectra using rhombic g tensors further supports the presence of a trigonal-bipyramidal active site (Fig. 3A, Hamiltonian parameters given in Table S1). The EPR spectrum of *SmAA10A* with cyanide show more axial g tensors (Fig. 3A). Compared to the spectrum without cyanide, the $A_{||}$ increases from 355 to 472 MHz, and the nitrogen superhyperfines become visible. This change in active site electronic geometry clearly indicates the influence of cyanide on Cu(II) and may indicate a transition towards a square planar active site.

As expected, considering the tetragonal conformation of the copper site and results of previous studies [64], *NcAA9C* has an axial EPR spectrum ($g_x = g_y \neq g_z$) in the absence of cyanide (Fig. 3B). The addition of cyanide has effects on the copper similar to those seen for *SmAA10A*. Cyanide increases the $A_{||}$ from 465 to 600 MHz, and the nitrogen superhyperfines become resolved.

The addition of cyanide to both enzymes resulted in the $m_1 = -3/2$ energy transition becoming visible, in line with the increased $^{63/65}\text{Cu}$ hyperfine distance ($A_{||}$).

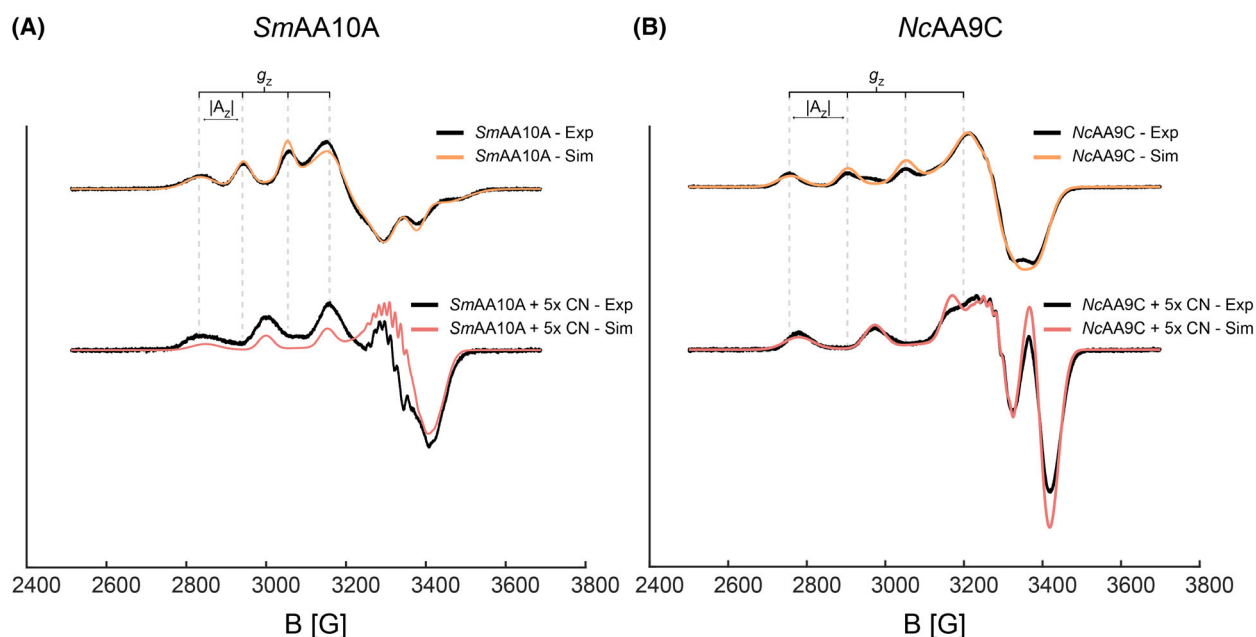


Fig. 3. CW X-band EPR spectroscopy. The spectra were collected on 400 μM SmAA10A (A) or NcAA9C (B), both in the absence and presence of 2 mM potassium cyanide. All samples were prepared in 50 mM MOPS, pH 7.0, and frozen in liquid nitrogen before collecting the spectra at 100 K. Data were collected using a sweep time of 60 s, modulation frequency of 100 kHz, modulation amplitude of 1 mT and microwave power of 10 mW. The raw data traces are black, and the simulations performed using the Easy Spin 6.0.0 Matlab package are presented in colors. Spin Hamiltonian parameters are shown in Table S1.

Simulations with and without cyanide yielded confident g_{\parallel} and A_{\parallel} values in the parallel region, however, lack of resolution in the perpendicular region excluded confident simulation of $A_{x,y}$ and $g_{x,y}$ values.

The effect of cyanide on substrate oxidation

The results reported above show that cyanide interacts with the active site copper of both LPMOs and that this interaction is stronger for NcAA9C compared to SmAA10A. Monitoring LPMO reactivity without substrate addresses off-pathway reactions that provide insight into LPMO copper reactivity. However, the physiologically relevant reaction occurs in the presence of a polysaccharide substrate. To investigate the effect of cyanide on catalysis, cyanide was added to reactions that were either *in situ* H_2O_2 -limiting or that were supplied with externally added H_2O_2 . Importantly, the time scales of these reactions are very different; for most of the reactions with externally added H_2O_2 reported below, the reaction was complete at the first of three reported measuring time points (i.e., after 3 min), whereas progress curves spanning multiple hours were obtained when using *in situ* H_2O_2 -limiting conditions.

Reactions of SmAA10A with β -chitin under *in situ* H_2O_2 -limiting conditions showed a slow release of oxidized products (Fig. 4A), which correlates with the low oxidase activity of this enzyme (Fig. 2B). Cyanide did not inhibit this reaction, which may seem strange in light of the impact of cyanide on the reduction of SmAA10A (Fig. 2F). However, under these conditions, substrate turnover is limited by *in situ* generation of H_2O_2 and, thus, is very slow (in the order of 0.002 s^{-1}), which means that the reduced reduction rate will not become rate-limiting. It is also worth noting that, considering the much higher rate of the peroxxygenase reaction (in the order of $1\text{--}10 \text{ s}^{-1}$; see below and [68]), only a minor fraction of reduced LPMO is needed to ensure immediate productive use of emerging H_2O_2 . Figure 4A shows that cyanide caused a slight increase in product formation after 24 h; similar minor boosting effects can be observed in several of the experiments shown hereafter and are discussed further below.

In contrast, in reactions driven by exogenously added H_2O_2 , cyanide inhibition became clearly visible at cyanide concentrations of 200 μM and higher (Fig. 4B). In these reactions, the reductant concentration is lower (100 μM), allowing the cyanide to better

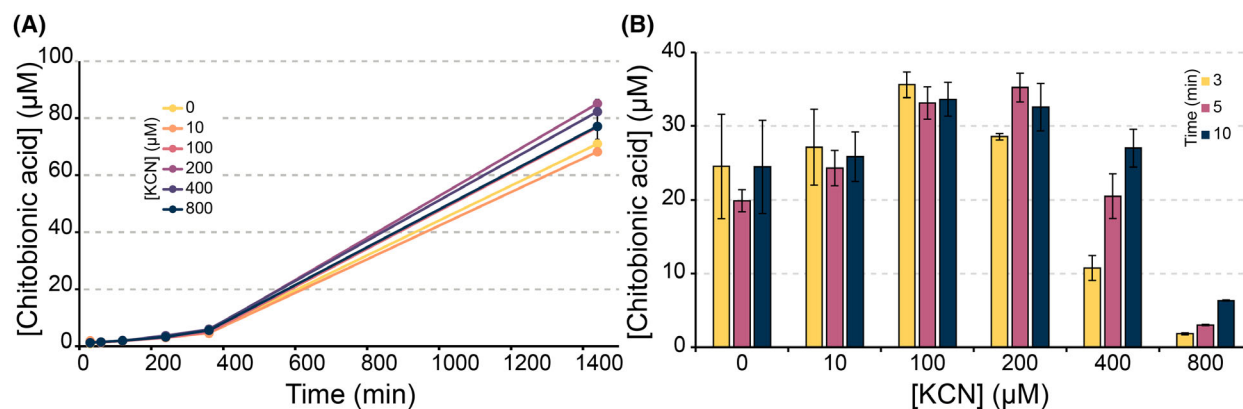


Fig. 4. Cyanide inhibition of chitin degradation by SmAA10A. (A) SmAA10A reactions were performed with 1 μM enzyme, 10 $\text{g}\cdot\text{L}^{-1}$ β -chitin and cyanide (0–800 μM) in 50 mM MOPS, pH 7.0, and initiated by adding 1 mM ascorbate (*in situ* H_2O_2 -limiting conditions). (B) SmAA10A reactions were performed with 1 μM enzyme, 10 $\text{g}\cdot\text{L}^{-1}$ β -chitin, cyanide (0–800 μM), and 100 μM exogenously added H_2O_2 in 50 mM MOPS, pH 7.0, and initiated by adding 100 μM ascorbate. For both reaction setups, soluble products were converted to native monomer (GlcNAc) and oxidized dimer (GlcNAcGlcNAc1A) and the latter was quantified. All reactions were performed in triplicates, standard deviations are shown as error bars.

compete with ascorbate and reduce the reduction rate. Furthermore, in these fast reactions, with a surplus of H_2O_2 , the concentration of active enzyme (i.e., reduced enzyme) will affect product formation, explaining why inhibition of reduction, in this case, translates into reduced product formation. Control reactions were performed to exclude an interaction between H_2O_2 and cyanide, showing that the concentration of H_2O_2 remains stable in the presence of cyanide (Fig. S4).

Similar to what was observed for SmAA10A, and despite more efficient inhibition of reduction by cyanide in the absence of substrate (Fig. 2F), reactions with NcAA9C acting on cellopentaose under *in situ* H_2O_2 -limiting conditions did not show inhibition of substrate conversion by cyanide. This underpins that reduction is not limiting the reaction under these conditions, as discussed above. Similar to the reactions with SmAA10A, the addition of cyanide, led to slightly increased product formation (Fig. 5A), which, in this case was accompanied by potential signs of enzyme inactivation (i.e., progress curves level off). These unexpected cyanide effects are addressed further in the Discussion section. To simplify interpretation of data, reaction setups with exogenously added H_2O_2 were used in subsequent experiments. Under these conditions, the oxidase activity will not be favored and, besides, the time frame of these reactions is so short that the effects of the slow oxidase reactions (and slow abiotic oxidation of the reductant) are expected to be small.

Interestingly, cyanide inhibition did not occur for NcAA9C acting on cellopentaose in reactions with 100 μM of exogenously added H_2O_2 (Fig. 5B), contrasting the results obtained with SmAA10A acting on chitin (Fig. 4B). It has been shown previously that conversion of small, soluble and easily diffusible cellopentaose by NcAA9C in reactions with added H_2O_2 is extremely efficient [27,69] and it is plausible that substrate interaction kinetics for this substrate are very different compared to an insoluble substrate. Efficient substrate binding will reduce off-pathway reoxidation of the enzyme through the peroxidase reaction, which will reduce the need for re-reduction as well as the impact of the inhibitory effect of cyanide on this reduction. Indeed, when using the insoluble substrate PASC, clear inhibition by cyanide did occur and full inhibition was observed at the higher concentrations (400–800 μM) (Fig. 5C). Notably, inhibition of NcAA9C acting on PASC happened at lower concentrations of cyanide compared to SmAA10A acting on chitin (Fig. 4B), in line with the stronger effect of cyanide on reduction of NcAA9C (Fig. 2F). Again, a small boosting effect of cyanide was observed at the lowest tested cyanide concentration (10 μM), which, notably, is some 10-fold lower than concentrations needed to slightly boost activity of SmAA10A. The observed inhibition shows that when using an insoluble, slow diffusing substrate, (re-)reduction of NcAA9C becomes a limiting factor and cyanide effects on reduction become noticeable. Taken together, the results so far show that the impact of cyanide on

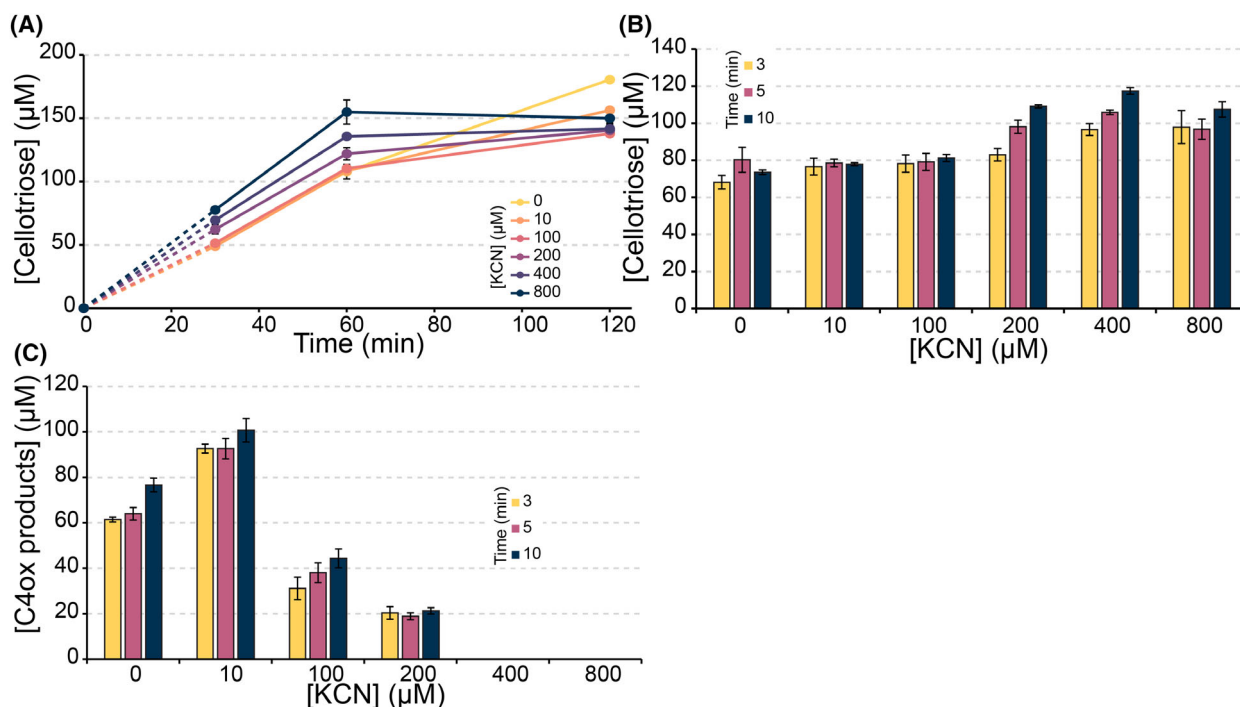


Fig. 5. Cyanide inhibition of the degradation of cellopentaose and PASC by *NcAA9C*. (A) *NcAA9C* reactions were performed with 1 μM enzyme, 1 mM cellopentaose and cyanide (0–800 μM) in 50 mM MOPS, pH 7.0, and initiated by adding 1 mM ascorbate. (B) *NcAA9C* peroxxygenase reactions were performed with 1 μM enzyme, 1 mM cellopentaose, 100 μM exogenously added H₂O₂, and 0–800 μM cyanide in 50 mM MOPS, pH 7.0, and initiated by adding 100 μM ascorbate. (C) *NcAA9C* reactions were performed with the same reaction conditions as in B; however, instead of 1 mM cellopentaose, 0.9% (w/v) PASC was used. For reactions performed using cellopentaose (A and B), cellotriose was quantified, whilst for reactions performed using PASC (C), the C4 oxidized dimer and trimer were quantified as described previously [57]. Standard deviations are shown as error bars ($n = 3$) for all reactions.

LPMO activity is both LPMO- and substrate-dependent.

The impact of reductant and substrate concentrations on LPMO inhibition

To further assess substrate and reductant effects in the inhibition of the LPMO reaction by cyanide, the concentrations of these components were varied in reactions with 0 or 200 μM cyanide. For *NcAA9C*, we focused on the reaction with cellopentaose, because the lack of cyanide inhibition of *NcAA9C* in reactions with 1 mM cellopentaose (Fig. 5A,B), contrasting with significant inhibition in reactions with PASC (Fig. 5C), warranted further investigation. Interestingly cyanide inhibition became detectable and increasingly prominent at lower cellopentaose concentrations (Fig. 6B). Likewise, inhibition by cyanide became visible at reductant concentrations below 100 μM, showing that reduction, and, thus, inhibition of reduction, became limiting (Fig. 6D).

Largely similar trends were observed for *SmAA10A*. Decreasing the concentration of the polymeric substrate β-chitin led to clearly increased inhibition by cyanide (Fig. 6A). Decreasing the reductant concentration in *SmAA10A* reactions had a more modest effect on cyanide inhibition compared to *NcAA9C* (Fig. 6C; compared with Fig. 6D), which aligns well with the lower impact of cyanide on the reduction rate (Fig. 2F). All in all, these results show that the inhibition of both *NcAA9C* and *SmAA10A* by cyanide depends on the substrate and the reductant concentration. Cyanide inhibition, caused by the interaction between cyanide and the oxidized LPMO [Cu(II) state], becomes more apparent as reductive activation becomes limiting in the LPMO reaction. This situation emerges at low reductant concentrations, but also at low substrate concentrations, since lack of substrate promotes oxidation of the LPMO through the off-pathway peroxidase reaction (i.e., futile turnover of H₂O₂), meaning that more frequent re-reduction is needed. The suitability and concentration of the substrate are important determinants of how LPMO

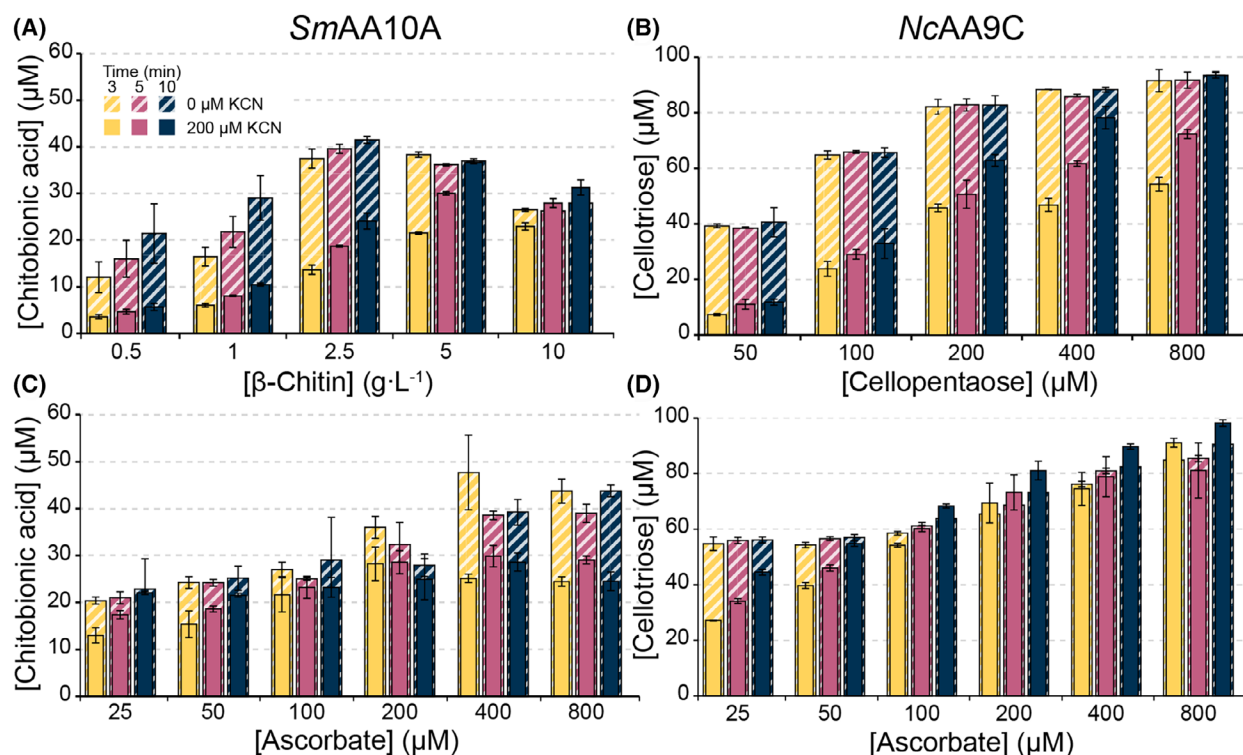


Fig. 6. The effect of substrate and reductant concentration on LPMO reactions. Substrate degradation was performed with 1 μM enzyme in 50 mM MOPS, pH 7.0, and 100 μM added H₂O₂, at 30 °C with 850 rpm agitation, varying either substrate or reductant concentration. Reactions were started by adding 100 μM ascorbate. For all reactions, time points were taken at 3, 5 and 10 min, and reactions were performed in the absence (striped bars) or presence of 200 μM cyanide (full-shaded bars). Panels A, C: *SmAA10A* reactions performed with (A) varying β-chitin concentrations (0.5–10 g·L⁻¹) with a fixed ascorbate concentration (100 μM) and (C) varying ascorbate concentrations (25–800 μM) with a fixed concentration of β-chitin (10 g·L⁻¹). Panels B, D: *NcAA9C* reactions with (B) varying cellopentaose concentrations (50–800 μM) with a fixed ascorbate concentration (100 μM) and (D) varying ascorbate concentrations (25–800 μM) with a fixed concentration of cellopentaose (1 mM). For reactions performed with *NcAA9C*, the cellotriose product was quantified using a Dionex ICS 6000 HPLC and for reactions performed with *SmAA10A* oxidized oligomers were degraded to the oxidized dimer (chitobionic acid), which was quantified using either a Dionex Ultimate 3000 UHPLC (A) or an Agilent 1290 UHPLC (C). All reactions were performed in triplicates, and standard deviations are shown as error bars for *n* = 3.

reactions proceed, not only in terms of inhibitor sensitivity, but also in terms of enzyme stability, since the peroxidase reaction may damage the enzyme [34,70].

Enzyme inactivation likely explains the peculiar effects observed when increasing the ascorbate concentration in the reaction with *SmAA10A* from the standard 100 μM to 400 and 800 μM. In these reactions, product formation increases considerably, and cyanide has a clear inhibitory effect that seems unexpected based on the above observation. We speculate that the increase in activity in the reactions without cyanide is due to the release of free copper by damaged enzymes, which will promote *in situ* generation of H₂O₂ through oxidation of ascorbate [41,42]. Cyanide could inhibit this effect by binding to copper in solution [71]. Previously published data show that enzyme inactivation

occurs for *SmAA10A* under the conditions used here [72] and that such inactivation indeed leads to copper release [42]. Control reactions showed that, indeed, cyanide inhibits LPMO reactions that are driven by copper-promoted oxidation of ascorbate (Fig. S5).

As an additional control, we also assessed why, for the *SmAA10A* reactions, the product yields are considerably lower than the 100 μM of product that could be generated when adding 100 μM H₂O₂ to the reaction. This low yield of soluble oxidized products (typically 30–40 μM) is expected to be due to the fact that a considerable fraction of LPMO-generated oxidized sites remain on the insoluble substrate [73]. Control reactions that include analysis of oxidized sites in the insoluble fraction indeed showed higher levels of oxidized products (Fig. S6).

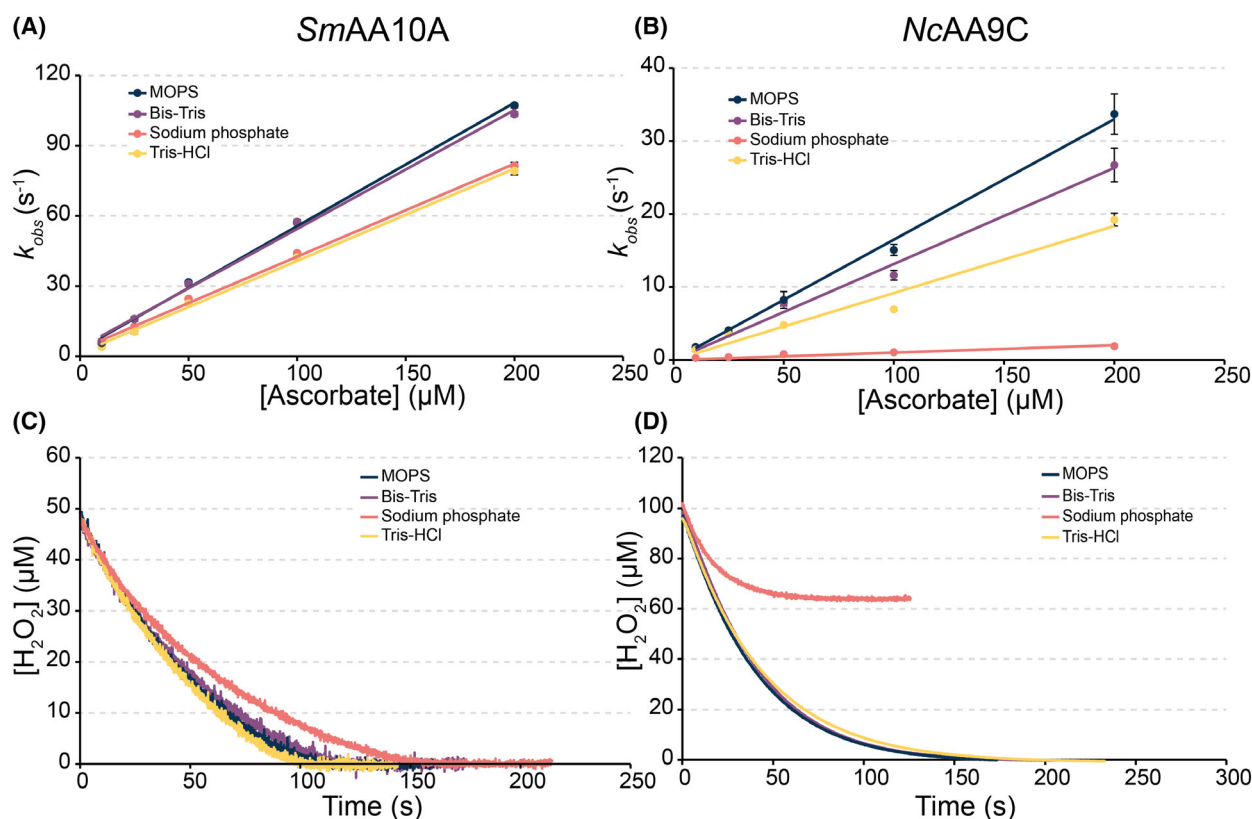


Fig. 7. The effect of different buffer molecules on LPMO reactivity. The rate of reduction for (A) *SmAA10A* and (B) *NcAA9C* was determined by stopped-flow mixing of $10 \mu M$ enzyme with increasing concentrations of ascorbate (10 – $200 \mu M$) in $50 mM$ buffer, pH 7.0. The observed rate (k_{obs}) was calculated using a single exponential equation $y = at + b + ce^{-kt}$ for each ascorbate concentration, and standard deviations are presented as error bars for $n = 3$. (C) Consumption of H_2O_2 by $1 \mu M$ *SmAA10A* acting on $10 g \cdot L^{-1}$ β -chitin in the presence of $50 \mu M$ H_2O_2 and after initiation of the reaction by adding $100 \mu M$ ascorbate. (D) Consumption of H_2O_2 by $50 nM$ *NcAA9C* acting on $4 g \cdot L^{-1}$ xyloglucan (XG) in the presence of $100 \mu M$ H_2O_2 and after initiation of the reaction by adding $100 \mu M$ ascorbate. The reactions depicted in panels C and D were done in $50 mM$ buffer, pH 7.0, containing $0.1 M$ KCl in triplicates, and one representative replicate was plotted. Second-order rate constants derived from panels A and B are listed in Tables S2 and S3. Initial rates derived from panels C and D are shown in Figs S8 and S9, respectively.

The impact of buffer ions on LPMO reactivity

Previous work has shown that organic acids and phosphoric acid inhibit the 2,6-DMP peroxidase reaction catalyzed by *NcAA9C* [47]. As expected, based on the above observations, cyanide clearly inhibited both *NcAA9C* and *SmAA10A* in the 2,6-DMP assay (Fig. S7), showing that this easy-to-use assay is useful for assessing a multitude of inhibitory effects.

Considering the huge difference between the two LPMOs in terms of the inhibition of reduction by cyanide (Fig. 2F), a negatively charged inhibitor, we then turned to the most prevalent charged molecule during LPMO reactions, namely the buffer molecule. Thus, we assessed the effect of sodium phosphate and different positively charged buffer molecules, using stopped-flow to monitor the effects on

reduction (Fig. 7A,B), an electrochemical sensor to measure the effects on H_2O_2 consumption in a reaction with the substrate (Fig. 7C,D) and the 2,6-DMP assay (Fig. 8).

The reduction rates for *SmAA10A* show modest buffer-dependent differences, with MOPS and Bis-Tris giving the highest reduction rates, followed by Tris/HCl and sodium phosphate (Fig. 7A; rates given in Table S2). Although there are differences in the reduction rate, these differences are limited and all rates far exceed the k_{cat} for the *SmAA10A* peroxygenase reaction with chitin ($6.7 s^{-1}$; [68]). It would thus seem that the variation in reduction rates will not significantly affect reactions with the substrate, as was indeed observed when monitoring the consumption of H_2O_2 in a reaction with β -chitin (Fig. 7C). All

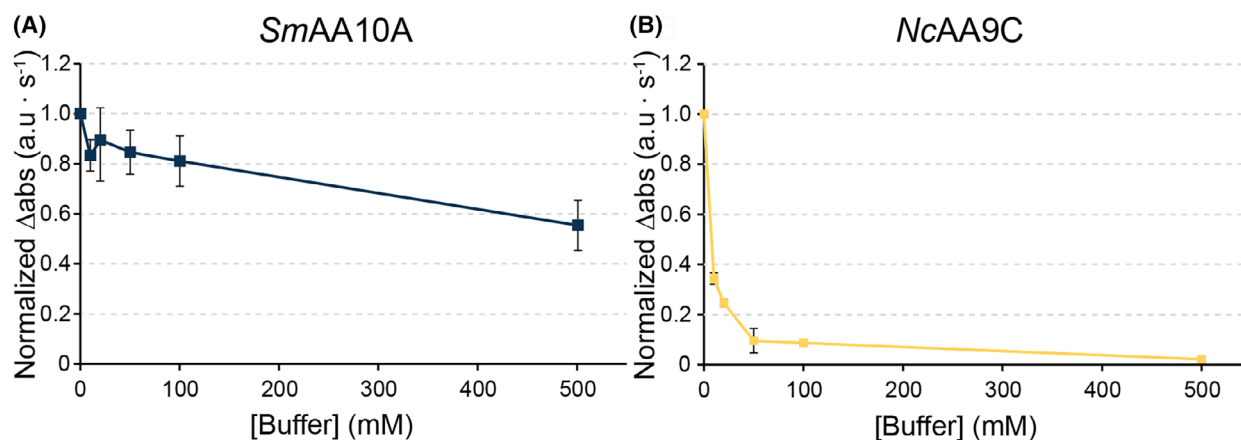


Fig. 8. Initial rates in the 2,6-DMP peroxidase reaction. Coerulignone formation was followed at 473 nm over time, and the linear portions of the reaction progress curves were used to determine the initial reaction rates, which were normalized. Reactions with *SmAA10A* (A) and *NcAA9C* (B) were prepared in 50 mM MOPS, pH 7.0, and the concentration of sodium phosphate was varied from 0 to 500 mM, and the pH was always 7.0. All reactions were performed in triplicates and standard deviations are presented as error bars for $n = 3$.

reactions showed similar initial rates (Fig. S8) and minimal differences in the progress curves (Fig. 7C).

While buffer effects for positively charged buffers were of similar magnitude for *NcAA9C*, strikingly, and in stark contrast to the above, reactions in sodium phosphate showed a 10-fold decrease in the reduction rate compared to MOPS (Fig. 7B). This, again, shows a big difference between the two LPMOs, in terms of the interaction of the copper site with negatively charged compounds. While such a buffer-dependent difference could become visible at low reductant or substrate concentrations (see above), the difference was not visible in the initial rates obtained from the H_2O_2 consumption assay (Fig. 7D), which were similar for all four buffers (Fig. S9). This assay was done with xyloglucan, which is an excellent soluble substrate for *NcAA9C* [27], with a more polymeric nature than cellopentaose. Xyloglucan could be used because the reaction is monitored by measuring H_2O_2 consumption, rather than by quantification of oxidized products, which is not possible for xyloglucan due to lack of standards.

Importantly, the H_2O_2 consumption assays with *NcAA9C* revealed another, unexpected difference between the buffers. The reactions in sodium phosphate suffered from fast enzyme inactivation, as suggested by the early flattening of the progress curve and the failure to consume all the H_2O_2 (Fig. 7D). Control reactions in which fresh enzyme was added after the termination of H_2O_2 consumption confirmed that enzyme inactivation indeed did occur, while the reaction mixture still contained both H_2O_2 and reductant (Fig. S10). It is conceivable that this early inactivation

relates to phosphate being a poor OH^\bullet radical quencher compared to the organic buffers. Indeed, a Fenton-like reaction in each of the tested buffers using the OH^\bullet specific radical trap terephthalic acid to detect OH^\bullet formation, only showed such formation for the reaction in sodium phosphate (Fig. S11).

To assess whether the observed differential impact of phosphate is specific for reactions with ascorbic acid, we also performed the 2,6-DMP peroxidase assay, which does not employ ascorbate. Figure 8 shows a trend similar to that observed during LPMO reduction (Fig. 7A,B): increasing the phosphate concentration had only a modest effect on the activity of *SmAA10A* whilst *NcAA9C* was severely affected.

Discussion

The results presented above show that cyanide inhibits LPMO catalysis. While this as such is not a surprising result, our exploration of cyanide inhibition revealed several important features of LPMO catalysis as well as potential pitfalls in the functional characterization of LPMOs. We show that cyanide inhibition may be easily overlooked, depending on the reaction conditions used, and we find a remarkable difference between an AA9 and an AA10 LPMO in terms of how well the enzyme interacts with the inhibitor. In addition, more or less serendipitously, we discovered that buffer ions may have huge effects on LPMO catalysis that, again, differ between LPMO types. The present results highlight the importance of understanding the multiple factors that govern LPMO catalysis. LPMOs require three reactants to perform a catalytic

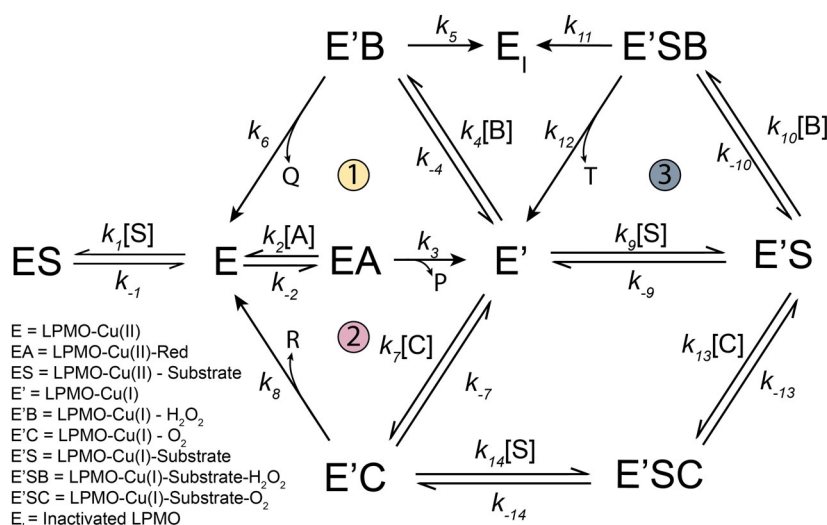


Fig. 9. King-Altman representation of LPMO catalysis. Double-sided arrows indicate reversible reactions, and single-sided arrows indicate non-reversible reactions. All second-order rates are converted to pseudo-first-order rates by adding the substrate concentrations (i.e., $k_2[A]$). Both substrate and product inhibition are disregarded, and enzyme-product complexes are omitted. During the LPMO reaction cycle, the copper active site is reduced from the resting Cu(II) state (E) to the active Cu(I) state (E'), which in turn can react with either O₂ (E'C, Path 1) or H₂O₂ (E'B, Path 2) in a substituted enzyme reaction [74,82]. In addition, LPMOs perform oxidative catalysis by binding both the polysaccharide substrate and H₂O₂ in a ternary complex reaction (E'SB, Path 3). The relative levels of different enzyme species will be affected by the presence of inhibitors such as cyanide. The reactants include A, B, C, and S, which are listed in the legend, and the various reactions lead to products P, Q, R, and T, which are oxidized reductant, water, H₂O₂ and oxidized substrate respectively.

turnover, the reductant, the co-substrate, and the polysaccharide substrate, but can also engage in multiple off-pathway reactions and may suffer from oxidative damage. The concentrations of the various substrates dictate the prevalence of reaction pathways and the balance of simultaneously occurring reactions, as illustrated by a King-Altman plot, adapted from [32], in Fig. 9.

The basic characterization of *SmAA10A* and *NcAA9C* shown in Fig. 2A–E is not novel [27,32,61,74], but comparing literature values can prove challenging due to varying laboratory conditions. Here the two enzymes were compared using the same methods and experimental conditions. Generally, the data (oxidase activity, rates of reduction by ascorbate and oxidation by H₂O₂, and activity in the 2,6-DMP assay) and the observed differences between the two LPMOs correspond well to literature data. *SmAA10A* has a higher reduction rate and a lower oxidation rate with both O₂ and H₂O₂ compared to *NcAA9C* in line with the higher reduction potential of the former [19,65,75]. The differences are likely not solely driven by the reduction potential as interactions with ascorbate, O₂, and H₂O₂ will also play a role. For example, analyzing the ascorbate peroxidase reaction for both *NcAA9C* and *SmAA10A*. Kuusk *et al.* showed that the enzymes have different K_m (AscA) and

K_m (H₂O₂) values [74]. As for H₂O₂ in the peroxidase reaction, *SmAA10A* has a K_m (H₂O₂) of $60 \pm 34 \mu\text{M}$, whereas *NcAA9C* has a K_m (H₂O₂) of $139 \pm 7 \mu\text{M}$ [74], while we show that the second-order rate constant for oxidation of reduced *NcAA9C* by H₂O₂ is some 10 times higher for the latter enzyme.

Our work with cyanide provides further insight into the differences between the two enzymes. The stopped-flow analyses of reduction clearly showed that cyanide inhibits reduction by ascorbate, suggesting binding of cyanide to the Cu(II). The EPR spectra of both *SmAA10A* and *NcAA9C* in the presence of cyanide confirmed Cu(II) – CN coordination. Similar changes in EPR spectra upon addition of cyanide, i.e., an increase in $A_{||}$ and resolved nitrogen superhyperfines, have been observed for other copper enzymes such as Cu-Zn superoxide dismutase [76], dopamine – β -monooxygenase [49,77] and galactose oxidase [78,79]. In addition, EPR spectra collected for an AA11 LPMO in the presence of azide also show a direct coordination with similar effects to $A_{||}$ [80]. Importantly, the EPR data show that cyanide binds to the Cu(II) state of the enzyme, in line with the notions that cyanide is a mimic of superoxide [76,81] and that LPMOs form Cu(II)-superoxide like intermediates [50,52]. The effects on reduction rates show that cyanide binds much stronger to *NcAA9C*-Cu(II) compared to *SmAA10A*-Cu(II).

To understand the observed impacts of cyanide one needs to consider several of the concentrations and rates shown in the King-Altman plot of Fig. 9, as alluded to above. For example, the lack of cyanide inhibition in *in situ* H₂O₂-limiting reactions for both enzymes is due to LPMO reduction not being rate-limiting. The theoretical reduction rates in the presence of the added surplus of ascorbate (1 mM) are in the order of 520 and 170 s⁻¹ (calculated from the second-order rates provided in Tables S2 and S3) for *SmAA10A* and *NcAA9C*, respectively. The rate of *in situ* H₂O₂-limiting LPMO reactions is on the min⁻¹ scale [40,69] and will, therefore, not be limited by inhibition of reduction by cyanide. On the other hand, in reactions with exogenously added H₂O₂, the lower ascorbate concentration (100 µM) leads to expected reduction rates of 52 and 17 s⁻¹ for *SmAA10A* and *NcAA9C* respectively. These reduction rates are close to reported enzymatic turnover numbers for H₂O₂-driven reactions [27,68,69], and, thus, cyanide inhibition becomes detectable. The type and concentration of the substrate also play major roles. If there is plenty, easily accessible substrate, the LPMO remains in the active Cu(I) state. The reaction will predominately follow path 3 (Fig. 9), whereas reoxidation of the enzyme to the Cu(II) state, the re-reduction of which would be inhibited by cyanide, is avoided. At lower effective substrate concentrations, paths 1 and 2 (oxidase and peroxidase side reactions, Fig. 9), each including a reduction reaction, will become more prominent, and the LPMO becomes susceptible to cyanide inhibition. The studies of the dependency of cyanide inhibition on the reductant concentration (Fig. 6) and the type (Fig. 5) and concentration (Fig. 6) of substrate support these considerations.

In some of the experiments described above, the presence of cyanide had unexpected minor positive effects on product formation. Further work is needed to rigorously explain these results, however two interesting and interconnected possible underlying causes stand out. Firstly, many of these observations can be explained by assuming that cyanide binding promotes the oxidase activity of LPMOs. Increased H₂O₂ production due to increased oxidase activity could explain the increased product yield. So far, the rate-limiting step in LPMO-catalyzed production of H₂O₂ has not been established and, besides, two reaction scenarios are being considered. In one of these, the superoxide resulting from reduction of O₂ by the LPMO-Cu(I) is released from the enzyme, followed by spontaneous disproportionation or a reductant-driven reaction to yield H₂O₂. Alternatively, H₂O₂ can be generated directly at the copper site, which

would require the supply of a second electron and two protons to the LPMO-Cu(II)-superoxide complex [83]. It is tempting to speculate that cyanide, being a superoxide mimic [76,81], could displace the Cu(II) bound superoxide and thus promote formation of H₂O₂ through the first scenario. This would imply that superoxide release is a rate-limiting step in the oxidase reaction.

The experimental data support this scenario, i.e., cyanide promoting release of superoxide from the LPMO, quite well. In *in situ* H₂O₂-limiting reactions, i.e. reactions that to a considerable extent depend on oxidase activity, cyanide leads to slightly increased product formation for both LPMOs (Figs 4A and 5A). This effect is stronger for *NcAA9C*, which is in perfect accordance with the stronger binding of cyanide for this enzyme. Figure 5A shows that increased initial rates in the presence of cyanide are accompanied by early onset of enzyme inactivation, which is typical for *in situ* H₂O₂-limiting reactions in which too much H₂O₂ is generated. Other evidence for the positive impact of cyanide on the oxidase activity comes from Fig. 5B showing degradation of cellopentaose in the presence of exogenously added H₂O₂. At 200 and 400 µM cyanide, the product levels of this reaction exceed the amount of added H₂O₂, which can only be explained by the *in situ* formation of additional H₂O₂. Of note, in this case product formation increases gradually over time, which is nicely compatible with the time scale of the *in situ* H₂O₂ limited reaction depicted in Fig. 5A.

Secondly, other effects may be at play, and promotion of the oxidase activity by cyanide cannot explain all the unexpected minor effects of cyanide on product formation. In several of the reactions, enzyme inactivation, which is accompanied by copper release [42], will take place. The release of free copper into a reductant-containing reaction mixture may lead to all sorts of reactions, including additional LPMO inactivation [43]. We suspect that some of the observed and not yet discussed unexpected cyanide effects relate to the proven (Fig. S5) impact of cyanide on the reactivity of free copper.

The higher affinity of *NcAA9C* for cyanide could potentially relate to an important difference in the second spheres of the two LPMOs studied here. A key second sphere residue in *SmAA10A* is a negatively charged glutamate known to coordinate H₂O₂ [18], whilst *NcAA9C* contains a neutral glutamine in an equivalent position [19]. It is conceivable that a negatively charged glutamate close to the active site repulses negatively charged cyanide, which could help explain why cyanide binds better to *NcAA9C*.

Interestingly, the higher affinity *NcAA9C* for cyanide was transferable to the negatively charged phosphate ion. When present at standard buffer concentrations, phosphate gave a 10-fold decrease in the reduction rate and led to inhibition in the ascorbate-independent 2,6-DMP peroxidase reaction. The lack of inhibition observed for *SmAA10A* by sodium phosphate again points towards different electronic structures in the active site. It is remarkable and important that commonly used buffers have such a strong impact on the functionality of *NcAA9C*.

Most remarkably, the experiments with various buffers revealed a huge effect of the buffer ion on the stability of *NcAA9C* in turnover conditions. Apparently, in phosphate buffer, *NcAA9C* is much more vulnerable to oxidative damage than in organic buffers. Organic buffers can react with radicals such as OH^\bullet , thus removing damaging oxidants from the solution [84,85]. On the other hand, sodium phosphate is commonly used in radical spin trapping experiments due to a lack of reactivity with radicals [86]. Control reactions with an OH^\bullet quencher indeed showed that OH^\bullet only accumulated in reactions with sodium phosphate. It may thus seem that the buffer affects radical formation and/or how well LPMOs can deal with such radicals. Perhaps, the buffer affects the efficiency of protective hole hopping pathways, that, notably, seem to differ between *SmAA10A* [72] and AA9 type LPMOs [87]. These intriguing observations, including the remarkable difference between *SmAA10A* and *NcAA9C*, warrant further studies and should serve as a cautionary tale for future LPMO research.

In conclusion, to the best of our knowledge, this is the first LPMO inhibition study presenting a quantitative investigation of both off-pathway and on-pathway LPMO reactions for two different LPMOs. The results and considerations presented above showcase the complexity of LPMO catalysis and the importance of understanding limiting factors during LPMO reactions. We show that cyanide binds the resting Cu(II) state LPMO, which results in inhibition during reaction conditions that involve formation of the Cu(II) state and that are limited by reduction of the enzyme. The complexity of LPMO reactions is due to the occurrence of several interconnected reactions at the same time, which are governed by the availability of the reductant, O_2 , H_2O_2 and the polysaccharide substrate. Our results reveal remarkable differences between the two studied LPMOs and it will be interesting to see if these differences are generally applicable to families of LPMOs with similar active site architectures. Finally, the here discovered LPMO-dependent large effects of the buffer ion on LPMO functionality warrant deeper

and wider follow-up studies that will be of major importance to the field.

Acknowledgements

This work was funded by the European Research Council (ERC) through the Horizon 2020 synergy project CUBE (Unraveling the secrets of Cu-based catalysts for C-H bond activation), grant number 856446, and by the Austrian Science Fund (FWF) Doctoral Program BioToP (Biomolecular Technology of Proteins), grant number W1224-B09. The authors acknowledge Ignacio Delgado Santamaria for preparing phosphoric acid swollen cellulose (PASC).

Author contributions

OG, LS, ZF, AAS and VGHE conceptualized and planned the experiments. OG, LS, TZE-M performed the experiments. OG, LS, ZF, AAS, TZE-M, KRH, IA-F, VGHE and ÅKR interpreted and discussed the data. OG and VGHE prepared the manuscript draft. MS and RL interpreted data. All authors discussed, edited and proof-read the manuscript.

Peer review

The peer review history for this article is available at <https://www.webofscience.com/api/gateway/wos/peer-review/10.1002/1873-3468.15105>.

Data availability

All underlying raw data is available in a public repository: <https://doi.org/10.18710/EBZKZQ>.

References

- 1 Hedegård ED and Ryde U (2017) Targeting the reactive intermediate in polysaccharide monooxygenases. *J Biol Inorg Chem* **22**, 1029–1037.
- 2 Ciano L, Davies GJ, Tolman WB and Walton PH (2018) Bracing copper for the catalytic oxidation of C–H bonds. *Nat Catal* **1**, 571–577.
- 3 Bissaro B and Eijsink VGH (2023) Lytic polysaccharide monooxygenases: enzymes for controlled and site-specific Fenton-like chemistry. *Essays Biochem* **67**, 575–584.
- 4 Hu J, Arantes V, Pribowo A and Saddler JN (2013) The synergistic action of accessory enzymes enhances the hydrolytic potential of a “cellulase mixture” but is highly substrate specific. *Biotechnol Biofuels* **6**, 112.
- 5 Cannella D, Hsieh C-WC, Felby C and Jørgensen H (2012) Production and effect of aldonic acids during

- enzymatic hydrolysis of lignocellulose at high dry matter content. *Biotechnol Biofuels* **5**, 26.
- 6 Müller G, Chylenski P, Bissaro B, Eijsink VGH and Horn SJ (2018) The impact of hydrogen peroxide supply on LPMO activity and overall saccharification efficiency of a commercial cellulase cocktail. *Biotechnol Biofuels* **11**, 209.
 - 7 Vaaje-Kolstad G, Westereng B, Horn SJ, Liu Z, Zhai H, Sørleie M and Eijsink VGH (2010) An oxidative enzyme boosting the enzymatic conversion of recalcitrant polysaccharides. *Science* **330**, 219–222.
 - 8 Vaaje-Kolstad G, Horn SJ, van Aalten DMF, Synstad B and Eijsink VGH (2005) The non-catalytic chitin-binding protein CBP21 from *Serratia marcescens* is essential for chitin degradation. *J Biol Chem* **280**, 28492–28497.
 - 9 Hemsworth GR, Johnston EM, Davies GJ and Walton PH (2015) Lytic polysaccharide monooxygenases in biomass conversion. *Trends Biotechnol* **33**, 747–761.
 - 10 Østby H, Hansen LD, Horn SJ, Eijsink VGH and Várnai A (2020) Enzymatic processing of lignocellulosic biomass: principles, recent advances and perspectives. *J Ind Microbiol Biotechnol* **47**, 623–657.
 - 11 Askarian F, Uchiyama S, Masson H, Sørensen HV, Golten O, Bunæs AC, Mekasha S, Røhr ÅK, Kommedal E, Ludviksen JA *et al.* (2021) The lytic polysaccharide monooxygenase CbpD promotes *Pseudomonas aeruginosa* virulence in systemic infection. *Nat Commun* **12**, 1230.
 - 12 Loose JSM, Forsberg Z, Fraaije MW, Eijsink VGH and Vaaje-Kolstad G (2014) A rapid quantitative activity assay shows that the *Vibrio cholerae* colonization factor GbpA is an active lytic polysaccharide monooxygenase. *FEBS Lett* **588**, 3435–3440.
 - 13 Yao RA, Reyre JL, Tamburrini KC, Haon M, Tranquet O, Nalubothula A, Mukherjee S, Le Gall S, Grisel S, Longhi S *et al.* (2023) The *Ustilago maydis* AA10 LPMO is active on fungal cell wall chitin. *Appl Environ Microbiol* **89**, e0057323.
 - 14 Sabbadin F, Urresti S, Henrissat B, Avrova AO, Welsh LRJ, Lindley PJ, Csukai M, Squires JN, Walton PH, Davies GJ *et al.* (2021) Secreted pectin monooxygenases drive plant infection by pathogenic oomycetes. *Science* **373**, 774–779.
 - 15 Qu M, Guo X, Tian S, Yang Q, Kim M, Mun S, Noh MY, Kramer KJ, Muthukrishnan S and Arakane Y (2022) AA15 lytic polysaccharide monooxygenase is required for efficient chitinous cuticle turnover during insect molting. *Commun Biol* **5**, 518.
 - 16 Zhong X, Zhang L, van Wezel GP, Vijgenboom E and Claessen D (2022) Role for a lytic polysaccharide monooxygenase in cell wall remodeling in *Streptomyces coelicolor*. *MBio* **13**, e0045622.
 - 17 Quinlan RJ, Sweeney MD, Leggio LL, Otten H, Poulsen J-CN, Johansen KS, Krogh KBRM, Jørgensen CI, Tovborg M, Anthonsen A *et al.* (2011) Insights into the oxidative degradation of cellulose by a copper metalloenzyme that exploits biomass components. *Proc Natl Acad Sci USA* **108**, 15079–15084.
 - 18 Bissaro B, Streit B, Isaksen I, Eijsink VGH, Beckham GT, DuBois JL and Røhr ÅK (2020) Molecular mechanism of the chitinolytic peroxxygenase reaction. *Proc Natl Acad Sci USA* **117**, 1504–1513.
 - 19 Hall KR, Joseph C, Ayuso-Fernandez I, Tamhankar A, Rieder L, Skaali R, Golten O, Neese F, Rohr AK, Jannuzzi SAV *et al.* (2023) A conserved second sphere residue tunes copper site reactivity in lytic polysaccharide monooxygenases. *J Am Chem Soc* **145**, 18888–18903.
 - 20 Vaaje-Kolstad G, Houston DR, Riemen AH, Eijsink VGH and van Aalten DM (2005) Crystal structure and binding properties of the *Serratia marcescens* chitin-binding protein CBP21. *J Biol Chem* **280**, 11313–11319.
 - 21 Span EA, Suess DLM, Deller MC, Britt RD and Marletta MA (2017) The role of the secondary coordination sphere in a fungal polysaccharide monooxygenase. *ACS Chem Biol* **12**, 1095–1103.
 - 22 Drula E, Garron M-L, Dogan S, Lombard V, Henrissat B and Terrapon N (2021) The carbohydrate-active enzyme database: functions and literature. *Nucleic Acids Res* **50**, D571–D577.
 - 23 Forsberg Z, Mackenzie AK, Sørleie M, Røhr ÅK, Helland R, Arvai AS, Vaaje-Kolstad G and Eijsink VGH (2014) Structural and functional characterization of a conserved pair of bacterial cellulose-oxidizing lytic polysaccharide monooxygenases. *Proc Natl Acad Sci USA* **111**, 8446–8451.
 - 24 Vu VV, Beeson WT, Span EA, Farquhar ER and Marletta MA (2014) A family of starch-active polysaccharide monooxygenases. *Proc Natl Acad Sci USA* **111**, 13822–13827.
 - 25 Frommhagen M, Sforza S, Westphal AH, Visser J, Hinz SW, Koetsier MJ, van Berkel WJ, Gruppen H and Kabel MA (2015) Discovery of the combined oxidative cleavage of plant xylan and cellulose by a new fungal polysaccharide monooxygenase. *Biotechnol Biofuels* **8**, 101.
 - 26 Sun P, Laurent CVFP, Boerkamp VJP, van Erven G, Ludwig R, van Berkel WJH and Kabel MA (2022) Regioselective C4 and C6 double oxidation of cellulose by lytic polysaccharide monooxygenases. *ChemSusChem* **15**, e202102203.
 - 27 Schwaiger L, Csarman F, Chang H, Golten O, Eijsink VGH and Ludwig R (2024) Electrochemical monitoring of heterogeneous peroxxygenase reactions unravels LPMO kinetics. *ACS Catal* **14**, 1205–1219.
 - 28 Danneels B, Tanghe M and Desmet T (2019) Structural features on the substrate-binding surface of fungal lytic

- polysaccharide monooxygenases determine their oxidative regioselectivity. *Biotechnol J* **14**, 1800211.
- 29 Tölgo M, Hegnar OA, Østby H, Várnai A, Vilaplana F, Eijsink VGH and Olsson L (2022) Comparison of six lytic polysaccharide monooxygenases from *Thermothielavioides terrestris* shows that functional variation underlies the multiplicity of LPMO genes in filamentous fungi. *Appl Environ Microbiol* **88**, e00096–22.
 - 30 Bennati-Granier C, Garajova S, Champion C, Grisel S, Haon M, Zhou S, Fanuel M, Ropartz D, Rogniaux H, Gimbert I *et al.* (2015) Substrate specificity and regioselectivity of fungal AA9 lytic polysaccharide monooxygenases secreted by *Podospira anserina*. *Biotechnol Biofuels* **8**, 90.
 - 31 Forsberg Z, Sørleie M, Petrović D, Courtade G, Aachmann FL, Vaaje-Kolstad G, Bissaro B, Røhr ÅK and Eijsink VGH (2019) Polysaccharide degradation by lytic polysaccharide monooxygenases. *Curr Opin Struct Biol* **59**, 54–64.
 - 32 Kuusk S, Kont R, Kuusk P, Heering A, Sørleie M, Bissaro B, Eijsink VGH and Väljamäe P (2019) Kinetic insights into the role of the reductant in H₂O₂-driven degradation of chitin by a bacterial lytic polysaccharide monooxygenase. *J Biol Chem* **294**, 1516–1528.
 - 33 Phillips CM, Beeson WT, Cate JH and Marletta MA (2011) Cellobiose dehydrogenase and a copper-dependent polysaccharide monooxygenase potentiate cellulose degradation by *Neurospora crassa*. *ACS Chem Biol* **6**, 1399–1406.
 - 34 Bissaro B, Røhr ÅK, Müller G, Chylenski P, Skaugen M, Forsberg Z, Horn SJ, Vaaje-Kolstad G and Eijsink VGH (2017) Oxidative cleavage of polysaccharides by monocopper enzymes depends on H₂O₂. *Nat Chem Biol* **13**, 1123–1128.
 - 35 Jones SM, Transue WJ, Meier KK, Kelemen B and Solomon EI (2020) Kinetic analysis of amino acid radicals formed in H₂O₂-driven Cu^I LPMO reoxidation implicates dominant homolytic reactivity. *Proc Natl Acad Sci USA* **117**, 11916–11922.
 - 36 Hedison TM, Breslmayr E, Shanmugam M, Karnpakdee K, Heyes DJ, Green AP, Ludwig R, Scrutton NS and Kracher D (2021) Insights into the H₂O₂-driven catalytic mechanism of fungal lytic polysaccharide monooxygenases. *FEBS J* **288**, 4115–4128.
 - 37 Kont R, Bissaro B, Eijsink VGH and Väljamäe P (2020) Kinetic insights into the peroxygenase activity of cellulose-active lytic polysaccharide monooxygenases (LPMOs). *Nat Commun* **11**, 5786.
 - 38 Chang H, Gacias Amengual N, Botz A, Schwaiger L, Kracher D, Scheiblbrandner S, Csarman F and Ludwig R (2022) Investigating lytic polysaccharide monooxygenase-assisted wood cell wall degradation with microsenors. *Nat Commun* **13**, 6258.
 - 39 Kittl R, Kracher D, Burgstaller D, Haltrich D and Ludwig R (2012) Production of four *Neurospora crassa* lytic polysaccharide monooxygenases in *Pichia pastoris* monitored by a fluorimetric assay. *Biotechnol Biofuels* **5**, 79.
 - 40 Golten O, Ayuso-Fernández I, Hall KR, Stepnov AA, Sørleie M, Røhr ÅK and Eijsink VGH (2023) Reductants fuel lytic polysaccharide monooxygenase activity in a pH-dependent manner. *FEBS Lett* **597**, 1363–1374.
 - 41 Stepnov AA, Forsberg Z, Sørleie M, Nguyen G-S, Wentzel A, Røhr ÅK and Eijsink VGH (2021) Unraveling the roles of the reductant and free copper ions in LPMO kinetics. *Biotechnol Biofuels* **14**, 28.
 - 42 Østby H, Tuveng TR, Stepnov AA, Vaaje-Kolstad G, Forsberg Z and Eijsink VGH (2023) Impact of copper saturation on lytic polysaccharide monooxygenase performance. *ACS Sustain Chem Eng* **11**, 15566–15576.
 - 43 Stepnov AA, Eijsink VGH and Forsberg Z (2022) Enhanced *in situ* H₂O₂ production explains synergy between an LPMO with a cellulose-binding domain and a single-domain LPMO. *Sci Rep* **12**, 6129.
 - 44 Rieder L, Petrović D, Väljamäe P, Eijsink VGH and Sørleie M (2021) Kinetic characterization of a putatively chitin-active LPMO reveals a preference for soluble substrates and absence of monooxygenase activity. *ACS Catal* **11**, 11685–11695.
 - 45 Tokin R, Frandsen KEH, Ipsen J, Lo Leggio L, Poojary MM, Berrin JG, Grisel S, Brander S, Jensen PE and Johansen KS (2021) Inhibition of lytic polysaccharide monooxygenase by natural plant extracts. *New Phytol* **232**, 1337–1349.
 - 46 Tokin R, Ipsen JØ, Poojary MM, Jensen PE, Olsson L and Johansen KS (2021) Inhibition of LPMOs by fermented persimmon juice. *Biomolecules* **11**, 1890.
 - 47 Breslmayr E, Poliak P, Požgajčić A, Schindler R, Kracher D, Oostenbrink C and Ludwig R (2022) Inhibition of the peroxygenase lytic polysaccharide monooxygenase by carboxylic acids and amino acids. *Antioxidants* **11**, 1096.
 - 48 Hasnain SS, Diakun GP, Knowles P, Binsted N, Garner C and Blackburn N (1984) Direct structural information for the copper site of dopamine beta-mono-oxygenase obtained by using extended X-ray-absorption fine structure. *Biochem J* **221**, 545–548.
 - 49 Blackburn NJ, Collison D, Sutton J and Mabbs FE (1984) Kinetic and e.p.r. studies of cyanide and azide binding to the copper sites of dopamine (3,4-dihydroxyphenethylamine) β-mono-oxygenase. *Biochem J* **220**, 447–454.
 - 50 Kjaergaard CH, Qayyum MF, Wong SD, Xu F, Hemsworth GR, Walton DJ, Young NA, Davies GJ, Walton PH, Johansen KS *et al.* (2014) Spectroscopic and computational insight into the activation of O₂ by the mononuclear Cu center in polysaccharide monooxygenases. *Proc Natl Acad Sci USA* **111**, 8797–8802.

- 51 Hedegård ED and Ryde U (2018) Molecular mechanism of lytic polysaccharide monooxygenases. *Chem Sci* **9**, 3866–3880.
- 52 Wang B, Wang Z, Davies GJ, Walton PH and Rovira C (2020) Activation of O₂ and H₂O₂ by lytic polysaccharide monooxygenases. *ACS Catal* **10**, 12760–12769.
- 53 Laurent CVFP, Sun P, Scheiblbrandner S, Csarman F, Cannazza P, Frommhagen M, van Berkel WJH, Oostenbrink C, Kabel MA and Ludwig R (2019) Influence of lytic polysaccharide monooxygenase active site segments on activity and affinity. *Int J Mol Sci* **20**, 6219.
- 54 Stepnov AA and Eijsink VGH (2023) Looking at LPMO reactions through the lens of the HRP/Ampex red assay. *Methods Enzymol* **679**, 163–189.
- 55 Wood TM (1988) Preparation of crystalline, amorphous, and dyed cellulose substrates. *Methods Enzymol* **160**, 19–25.
- 56 Heuts DPHM, Winter RT, Damsma GE, Janssen DB and Fraaije MW (2008) The role of double covalent flavin binding in chito-oligosaccharide oxidase from *Fusarium graminearum*. *Biochem J* **413**, 175–183.
- 57 Østby H, Jameson J-K, Costa T, Eijsink VGH and Arntzen MØ (2022) Chromatographic analysis of oxidized cello-oligomers generated by lytic polysaccharide monooxygenases using dual electrolytic eluent generation. *J Chromatogr A* **1662**, 462691.
- 58 Bissaro B, Forsberg Z, Ni Y, Hollmann F, Vaaje-Kolstad G and Eijsink VGH (2016) Fueling biomass-degrading oxidative enzymes by light-driven water oxidation. *Green Chem* **18**, 5357–5366.
- 59 Breslmayr E, Hanžek M, Hanrahan A, Leitner C, Kittl R, Šantek B, Oostenbrink C and Ludwig R (2018) A fast and sensitive activity assay for lytic polysaccharide monooxygenase. *Biotechnol Biofuels* **11**, 79.
- 60 Stoll S and Schweiger A (2006) EasySpin, a comprehensive software package for spectral simulation and analysis in EPR. *J Magn Reson* **178**, 42–55.
- 61 Isaksen T, Westereng B, Aachmann FL, Agger JW, Kracher D, Kittl R, Ludwig R, Haltrich D, Eijsink VGH and Horn SJ (2014) A C4-oxidizing lytic polysaccharide monooxygenase cleaving both cellulose and cello-oligosaccharides. *J Biol Chem* **289**, 2632–2642.
- 62 Agger JW, Isaksen T, Várnai A, Vidal-Melgosa S, Willats WG, Ludwig R, Horn SJ, Eijsink VGH and Westereng B (2014) Discovery of LPMO activity on hemicelluloses shows the importance of oxidative processes in plant cell wall degradation. *Proc Natl Acad Sci USA* **111**, 6287–6292.
- 63 Forsberg Z, Røhr ÅK, Mekasha S, Andersson KK, Eijsink VGH, Vaaje-Kolstad G and Sørle M (2014) Comparative study of two chitin-active and two cellulose-active AA10-type lytic polysaccharide monooxygenases. *Biochemistry* **53**, 1647–1656.
- 64 Borisova AS, Isaksen T, Dimarogona M, Kognole AA, Mathiesen G, Várnai A, Røhr ÅK, Payne CM, Sørle M, Sandgren M *et al.* (2015) Structural and functional characterization of a lytic polysaccharide monooxygenase with broad substrate specificity. *J Biol Chem* **290**, 22955–22969.
- 65 Aachmann FL, Sørle M, Skjåk-Bræk G, Eijsink VGH and Vaaje-Kolstad G (2012) NMR structure of a lytic polysaccharide monooxygenase provides insight into copper binding, protein dynamics, and substrate interactions. *Proc Natl Acad Sci USA* **109**, 18779–18784.
- 66 Lindley PJ, Parkin A, Davies GJ and Walton PH (2022) Mapping the protonation states of the histidine brace in an AA10 lytic polysaccharide monooxygenase using CW-EPR spectroscopy and DFT calculations. *Faraday Discuss* **234**, 336–348.
- 67 Forsberg Z, Nelson CE, Dalhus B, Mekasha S, Loose JSM, Crouch LI, Røhr ÅK, Gardner JG, Eijsink VGH and Vaaje-Kolstad G (2016) Structural and functional analysis of a lytic polysaccharide monooxygenase important for efficient utilization of chitin in *Cellvibrio japonicus*. *J Biol Chem* **291**, 7300–7312.
- 68 Kuusk S, Bissaro B, Kuusk P, Forsberg Z, Eijsink VGH, Sørle M and Väljamäe P (2018) Kinetics of H₂O₂-driven degradation of chitin by a bacterial lytic polysaccharide monooxygenase. *J Biol Chem* **293**, 523–531.
- 69 Rieder L, Stepnov AA, Sørle M and Eijsink VGH (2021) Fast and specific peroxygenase reactions catalyzed by fungal mono-copper enzymes. *Biochemistry* **60**, 3633–3643.
- 70 Loose JSM, Arntzen MØ, Bissaro B, Ludwig R, Eijsink VGH and Vaaje-Kolstad G (2018) Multipoint precision binding of substrate protects lytic polysaccharide monooxygenases from self-destructive off-pathway processes. *Biochemistry* **57**, 4114–4124.
- 71 Lu J, Dreisinger DB and Cooper WC (2002) Thermodynamics of the aqueous copper–cyanide system. *Hydrometallurgy* **66**, 23–36.
- 72 Ayuso-Fernández I, Emrich-Mills TZ, Haak J, Golten O, Hall KR, Schwaiger L, Moe TS, Stepnov AA, Ludwig R, Cutsail Iii GE *et al.* (2024) Mutational dissection of a hole hopping route in a lytic polysaccharide monooxygenase (LPMO). *Nat Commun* **15**, 3975.
- 73 Kracher D, Forsberg Z, Bissaro B, Gangl S, Preims M, Sygmund C, Eijsink VGH and Ludwig R (2020) Polysaccharide oxidation by lytic polysaccharide monooxygenase is enhanced by engineered cellobiose dehydrogenase. *FEBS J* **287**, 897–908.
- 74 Kuusk S, Eijsink VGH and Väljamäe P (2023) The “life-span” of lytic polysaccharide monooxygenases (LPMOs) correlates to the number of turnovers in the reductant peroxidase reaction. *J Biol Chem* **299**, 105094.

- 75 Munzone A, Pujol M, Tamhankar A, Joseph C, Mazurenko I, Réglier M, Jannuzzi SAV, Royant A, Sicoli G, DeBeer S *et al.* (2024) Integrated experimental and theoretical investigation of copper active site properties of a lytic polysaccharide monooxygenase from *Serratia marcescens*. *Inorg Chem* **63**, 11063–11078.
- 76 Paci M, Desideri A and Rotilio G (1988) Cyanide binding to Cu, Zn superoxide dismutase. An NMR study of the Cu(II), Co(II) derivative. *J Biol Chem* **263**, 162–166.
- 77 Obata A, Tanaka H and Kawazura H (1987) Magnetic resonance studies on the copper site of dopamine. Beta.-monooxygenase in the presence of cyanide and azide anions. *Biochemistry* **26**, 4962–4968.
- 78 Marwedel BJ, Kosman DJ, Bereman RD and Kurland RJ (1981) Magnetic resonance studies of cyanide and fluoride binding to galactose oxidase copper(II): evidence for two exogenous ligand sites. *J Am Chem Soc* **103**, 2842–2847.
- 79 Whittaker MM and Whittaker JW (1993) Ligand interactions with galactose oxidase: mechanistic insights. *Biophys J* **64**, 762–772.
- 80 Hemsworth GR, Henrissat B, Davies GJ and Walton PH (2014) Discovery and characterization of a new family of lytic polysaccharide monooxygenases. *Nat Chem Biol* **10**, 122–126.
- 81 Shearer J, Fitch SB, Kaminsky W, Benedict J, Scarrow RC and Kovacs JA (2003) How does cyanide inhibit superoxide reductase? Insight from synthetic $\text{Fe}^{\text{III}}\text{N}_4\text{S}$ model complexes. *Proc Natl Acad Sci USA* **100**, 3671–3676.
- 82 Cornish-Bowden A (2012) Fundamentals of Enzyme Kinetics. 4th edn. Wiley-Blackwell, Hoboken, NJ.
- 83 Wang B, Walton PH and Rovira C (2019) Molecular mechanisms of oxygen activation and hydrogen peroxide formation in lytic polysaccharide monooxygenases. *ACS Catal* **9**, 4958–4969.
- 84 Hicks M and Gebicki JM (1986) Rate constants for reaction of hydroxyl radicals with Tris, Tricine and Hepes buffers. *FEBS Lett* **199**, 92–94.
- 85 Shiraishi H, Kataoka M, Morita Y and Umemoto J (1993) Interactions of hydroxyl radicals with tris (hydroxymethyl) aminomethane and Good's buffers containing hydroxymethyl or hydroxyethyl residues produce formaldehyde. *Free Radic Res Commun* **19**, 315–321.
- 86 Janzen EG, Kotake Y and Randall DH (1992) Stabilities of hydroxyl radical spin adducts of PBN-type spin traps. *Free Radic Biol Med* **12**, 169–173.
- 87 Zhao J, Zhuo Y, Diaz DE, Shanmugam M, Telfer AJ, Lindley PJ, Kracher D, Hayashi T, Seibt LS, Hardy FJ *et al.* (2023) Mapping the initial stages of a protective pathway that enhances catalytic turnover by a lytic polysaccharide monooxygenase. *J Am Chem Soc* **145**, 20672–20682.

Supporting information

Additional supporting information may be found online in the Supporting Information section at the end of the article.

Fig. S1. Workflow and data treatment when measuring H_2O_2 consumption with the electrochemical sensor.

Fig. S2. Stopped-flow control reactions comparing LPMO reduction with ascorbate or cyanide.

Fig. S3. Cyanide as a possible reductant in *SmAA10A* reactions.

Fig. S4. H_2O_2 stability in the presence of KCN.

Fig. S5. Effect of cyanide on the activity of *SmAA10A* in *in situ* H_2O_2 -limiting reactions that contain free copper.

Fig. S6. Product formation by *SmAA10A*.

Fig. S7. Inhibition of 2,6-DMP oxidation by cyanide.

Fig. S8. Turnover numbers for *SmAA10A* acting on β -chitin in various buffers.

Fig. S9. Turnover numbers for *NcAA9C* acting on xyloglucan in various buffers.

Fig. S10. H_2O_2 consumption by *NcAA9C* acting on xyloglucan in a phosphate buffer monitored with an electrochemical sensor.

Fig. S11. Formation of OH^\bullet radicals in various buffers.

Table S1. Spin Hamiltonian parameters of LPMOs in the absence and presence of cyanide.

Table S2. Second-order reduction rates for *SmAA10A* in varying buffers (50 mM, pH 7.0) with 100 μM ascorbate.

Table S3. Second-order reduction rates for *NcAA9C* in varying buffers (50 mM, pH 7.0) with 100 μM ascorbate.